AGU ADVANCING EARTH AND SPACE SCIENCES

JAMES | Journal of Advances in Modeling Earth Systems®

RESEARCH ARTICLE
10.1029/2025MS005257

Modeling Sub-Grid Peatland Vegetation Dynamics in the ORCHIDEE-PEAT Land Surface Model

Chunjing Qiu[1,2,3], Philippe Ciais[3], Chenyu Bian[1,2], Liyang Liu[3], Bertrand Guenet[4], Dan Zhu[5,6], Xinyu Chen[1,2], Chengliuhui Fang[1,2], Jianyang Xia[1,2], Anna M. Peregon[7], Natalia P. Kosykh[8], Nina P. Mironycheva–Tokareva[8], Jiří Dušek[9], Efrén López-Blanco[10,11], Jingfeng Xiao[12], Xing Li[13], Ankur R. Desai[14], Eugénie Euskirchen[15], Colin Edgar[15], Joshua Ratcliffe[16,17], Matthias Peichl[17], Koffi Dodji Noumonvi[17], Krzysztof Fortuniak[18], Włodzimierz Pawlak[18], Annalea Lohila[19,20], Mika Korkiakoski[19], Mika Aurela[19], and Aram Kalhori[21,22]

[1]Research Center for Global Change and Ecological Forecasting, School of Ecological and Environmental Sciences, East China Normal University, Shanghai, China, [2]Institute of Eco-Chongming, East China Normal University, Shanghai, China, [3]Laboratoire des Sciences du Climat et de l'Environnement (LSCE), CEA–CNRS– UVSQ, IPSL, Université Paris-Saclay, Gif-sur-Yvette, France, [4]LG-ENS (Laboratoire de Géologie) CNRS UMR 8538—Ecole Normale Supérieure, PSL University —IPSL, Paris, France, [5]Sino-French Institute for Earth System Science, College of Urban and Environmental Sciences, Peking University, Beijing, China, [6]Institute of Carbon Neutrality, Peking University, Beijing, China, [7]Science Partners, Paris, France, [8]Institute of Soil Science and Agrochemistry, Siberian Branch of the Russian Academy of Sciences (ISSA SB RAS), Novosibirsk, Russia, [9]Global Change Research Institute of the Czech Academy of Sciences, Brno, Czech Republic, [10]Department of Ecoscience and Arctic Research Centre, Aarhus University, Roskilde, Denmark, [11]Department of Environment and Minerals, Greenland Institute of Natural Resources, Nuuk, Greenland, [12]Earth Systems Research Center, Institute for the Study of Earth, Oceans, and Space, University of New Hampshire, Durham, NH, USA, [13]School of Geography and Planning, Sun Yat-sen University, Guangzhou, China, [14]Department of Atmospheric and Oceanic Sciences, University of Wisconsin-Madison, Madison, WI, USA, [15]Institute of Arctic Biology, University of Alaska Fairbanks, Fairbanks, AK, USA, [16]Unit for Field-Based Forest Research, Swedish University of Agricultural Sciences, Vindeln, Sweden, [17]Department of Forest Ecology and Management, Swedish University of Agricultural Sciences, Umeå, Sweden, [18]Faculty of Geographical Sciences, Department of Meteorology and Climatology, University of Lodz, Lodz, Poland, [19]Finnish Meteorological Institute, Helsinki, Finland, [20]INAR/Physics, University of Helsinki, Helsinki, Finland, [21]GFZ Helmholtz Centre for Geosciences, Potsdam, Germany, [22]Michael Succow Foundation, Partner in the Greifswald Mire Centre, Greifswald, Germany

Abstract Peatlands store about one-third of total global soil carbon. Vegetation composition strongly regulates peatland carbon dynamics. Global warming and climate-driven ecohydrological changes are expected to alter peatland vegetation composition, necessitating accurate simulation of vegetation dynamics to predict future fate of peatland carbon. We incorporated six plant functional types (PFTs) into the ORCHIDEE-PEAT model to represent bryophytes (mosses), C3 graminoids (sedges and grasses), boreal broadleaf deciduous shrubs, boreal needleleaf evergreen trees, tropical evergreen and raingreen (water-driven deciduous) trees growing in peatlands. The introduction and elimination of each PFT in response to bioclimatic conditions, as well as sapling establishment, growth, mortality, and competition among PFTs, are explicitly modeled. Simulated vegetation distributions align well with site-level observations from West Siberian wetlands, where extensive vegetation composition measurements are available for model evaluation. The model slightly overestimated gross primary productivity (GPP) across 60 sites. Evaluation using global satellite-derived land cover, leaf area index and GPP data was encouraging, though challenges lie in the lack of observational data specific to peatlands. From 1901 to 2020, simulated tropical peatland vegetation composition remains relatively stable. In northern peatlands, as a result of warming and declining water table, bryophyte and C3 graminoid cover decrease by 0.2 (13%) and 0.1 (13%) million km^2, respectively, while shrub and tree cover increase by 0.3 (75%) and 0.03 (2%) million km^2, respectively. The impacts of these vegetation shift on peatland carbon balance can be explored in future studies using the model, which integrates peatland vegetation dynamics with peatland-specific hydrology and carbon cycling.

Plain Language Summary Peatlands are a type of wetlands that store large amounts of carbon in their soils. Natural peatlands remove carbon dioxide from the atmosphere, but they also release methane, another powerful greenhouse gas. Whether peatlands act overall as a source or sink of greenhouse gases depends on the balance between carbon dioxide uptake by plants and the release of carbon dioxide and methane from the

Key Points:

- The representation of peatland vegetation in the ORCHIDEE-PEAT model is improved by adding bryophytes, C3 graminoids, shrubs, and trees
- The spatial distribution of peatland vegetation is dynamically simulated based on their interactions and climate
- The model simulated shrubification and woody encroachment in northern peatlands from 1901 to 2020

Supporting Information:

Supporting Information may be found in the online version of this article.

Correspondence to:

C. Qiu,
cjqiu@des.ecnu.edu.cn

Citation:

Qiu, C., Ciais, P., Bian, C., Liu, L., Guenet, B., Zhu, D., et al. (2026). Modeling sub-grid peatland vegetation dynamics in the ORCHIDEE-PEAT land surface model. *Journal of Advances in Modeling Earth Systems*, *18*, e2025MS005257. https://doi.org/10.1029/2025MS005257

Received 4 JUN 2025
Accepted 27 FEB 2026

Author Contributions:

Conceptualization: Chunjing Qiu
Data curation: Chenyu Bian, Xinyu Chen, Anna M. Peregon, Natalia P. Kosykh, Nina P. Mironycheva–Tokareva, Jiří Dušek, Efrén López-Blanco, Jingfeng Xiao, Xing Li, Ankur R. Desai, Eugénie Euskirchen, Colin Edgar, Joshua Ratcliffe, Matthias Peichl, Koffi Dodji Noumonvi, Krzysztof Fortuniak, Włodzimierz Pawlak, Annalea Lohila, Mika Korkiakoski, Mika Aurela, Aram Kalhori
Formal analysis: Chunjing Qiu
Funding acquisition: Jianyang Xia

Methodology: Chunjing Qiu, Philippe Ciais
Software: Chunjing Qiu, Liyang Liu, Dan Zhu
Writing – original draft: Chunjing Qiu
Writing – review & editing: Chunjing Qiu, Philippe Ciais, Chenyu Bian, Liyang Liu, Bertrand Guenet, Dan Zhu, Xinyu Chen, Chengliuhui Fang, Jianyang Xia, Anna M. Peregon, Natalia P. Kosykh, Nina P. Mironycheva–Tokareva, Jiří Dušek, Efrén López-Blanco, Jingfeng Xiao, Xing Li, Ankur R. Desai, Eugénie Euskirchen, Colin Edgar, Joshua Ratcliffe, Matthias Peichl, Koffi Dodji Noumonvi, Krzysztof Fortuniak, Włodzimierz Pawlak, Annalea Lohila, Mika Korkiakoski, Mika Aurela, Aram Kalhori

soil. To better represent these processes, we included bryophytes, C3 graminoids, shrubs, and trees in the ORCHIDEE-PEAT model to account for the diversity of peatland vegetation types and their competitive interactions. We evaluated the model by comparing its simulated plant distribution and carbon uptake with observation-based estimates. The model suggests that from 1901 to 2020, peatlands in the Northern Hemisphere experienced changes in plant communities: the coverage of peatland bryophytes and C3 graminoids decreased, while the coverage of peatland shrubs and trees increased. In tropical regions, peatland vegetation changed little. This model provides a useful tool for studying how changes in plant communities may affect peatland greenhouse gases and how peatlands may influence the global climate system.

1. Introduction

In recent decades, widespread greening of the Earth has occurred in response to climate warming and elevated CO_2 concentrations. This has been well documented by satellite data, and to an extent confirmed also by increased productivity observed from field observations, and warming experiments (Frost et al., 2025; Jeong et al., 2024; Piao et al., 2020; Zhu et al., 2016). It signifies various changes, including increase in vegetation height, leaf area and biomass, as well as shifts in vegetation composition (e.g., shrubification of arctic and sub-arctic tundra) and phenology (Bjorkman et al., 2018, 2020; Mekonnen et al., 2021; Myers-Smith et al., 2020; Piao et al., 2020; Zhu et al., 2016).

Northern high latitude regions, containing the largest expanse of peatlands in the world, have been warming much faster than elsewhere (Rantanen et al., 2022). Natural peatlands, which store approximately one third of the world's soil carbon (Ribeiro et al., 2021), are also important CO_2 sinks and CH_4 sources, with the cooling effect of CO_2 uptake offsetting the warming effect of CH_4 emissions, leading to a net cooling effect on the climate system (Frolking & Roulet, 2007; Leifeld & Menichetti, 2018). However, recent climate change and human activities have caused significant hydrological shifts in peatlands. For example, a widespread drying has been observed in European peatlands in recent centuries (Swindles et al., 2019), whereas in northeastern Canada peatlands, a wetting trend was more frequently observed (Zhang et al., 2022). Warmer climate and hydrological changes can induce changes in the composition of peatland vegetation. Different types of peatlands (e.g., ombrotrophic bogs and minerotrophic fens) and plant species may respond differently, but the general trend is a shift from the prevalent non-vascular *Sphagnum* mosses toward a greater abundance of vascular plants in response to rising temperatures (Dieleman et al., 2015; McPartland et al., 2020; Norby et al., 2019; Weltzin et al., 2003) and declining water table levels (Jassey et al., 2018).

Shifts in peatland vegetation composition can alter the capacity of peatlands to function as CO_2 sinks and CH_4 sources (Bragazza et al., 2013; Gavazov et al., 2018; Goud et al., 2017; Kalhori et al., 2024; Mekonnen et al., 2021; Ratcliffe et al., 2020; Wang et al., 2015). However, our knowledge about peatland vegetation changes at large scales remains limited. The fine-scale spatial complexity of peatlands (i.e., intricate variations in peatland topography and hydrology leading to distinct vegetation compositions in the hummock-lawn-hollow micro-topography) poses significant challenges for accurately classifying peatland vegetation mixtures using remotely sensed data and common mapping techniques (Räsänen et al., 2020). In addition, remote sensing faces significant challenges when dealing with dense vegetation (e.g., paludified forests in boreal North America and lowland tropical peatlands, which are typically covered by dense swamp forests) and is hindered by contamination from clouds and aerosols (Piao et al., 2020).

Process-based models are valuable tools for understanding and predicting vegetation dynamics in ecosystems, accounting for the interactions between vegetation, hydrological processes and carbon fluxes. However, peatlands are complex adaptive systems that are challenging to model (Belyea & Baird, 2006). To date, peatlands have been incorporated into many process-based land surface models (Chadburn et al., 2022; Chaudhary et al., 2017; Kleinen et al., 2012; Müller & Joos, 2020; Qiu et al., 2018; Shi et al., 2021; Zhao & Zhuang, 2023). Nevertheless, many existing models have limitations in representing the complexity of peatlands and accurately capturing their responses to climate forcings (Qiu et al., 2022). A major source of the complexity in peatland responses to climate is vegetation feedbacks. The representation of peatland vegetation in models ranges from those that include only non-woody vegetation types such as mosses and graminoids (Qiu et al., 2018; Wania et al., 2009), to those that also incorporate shrubs and trees (Chaudhary et al., 2017; Müller & Joos, 2020; Zhao & Zhuang, 2023). In the

state-of-the-art land surface model, ORCHIDEE-PEAT, peatland-specific hydrology and water table dynamics (Qiu et al., 2018), and their coupling with the carbon cycle (Kwon et al., 2022; Qiu et al., 2019; Salmon et al., 2022) are explicitly modeled. However, the parameterization of peatland vegetation in the model has been relatively simple - it uses only one grass-like plant functional type (PFT) to represent the average vegetation growing in intact northern peatlands. This approach overlooks the diversity of vegetation growth forms and their distinct responses to climate change. Moreover, it hinders the model's applicability to tropical peatlands, which are typically characterized by dense trees rather than herbaceous vegetation. To address this limitation, we enhanced the representation of peatland vegetation by incorporating multiple peatland-specific PFTs, including bryophytes, C3 graminoids (using the characteristic parameters of the grass-like PFT from ORCHIDEE-PEAT), shrubs, and trees (Section 2.2).

The fractional area covered by each PFT within a grid cell can be prescribed from vegetation/land cover maps or dynamically simulated using the vegetation dynamics module. The vegetation dynamics module in ORCHIDEE-PEAT was adapted from the LPJ model (Krinner et al., 2005; Sitch et al., 2003) and further improved by Zhu et al. (2015). Vegetation dynamics are determined by the balance between sapling establishment and plant death caused by natural mortality (background mortality, extreme coldness-induced mortality and spring frost-induced mortality for trees), competition between PFTs, and disturbances. However, the module does not differentiate peatlands from upland ecosystems, thus the establishment and death of plants are constrained by the grid cell mean bioclimatic conditions, and non-peat PFTs compete with peat PFTs for light and space. In light of the differences between peatlands and upland ecosystems, marked by the presence of water at or near the soil surface and the thriving of specialized plants in such conditions, we revised the vegetation dynamics module to separate peatlands and upland ecosystems (Section 2.3). Vegetation dynamics of peatlands are now independently simulated and fully coupled with peatland-specific hydrology and carbon cycle modules. The results of the model are evaluated using global satellite-derived land cover map, GPP and LAI products, as well as site-level measurements of vegetation cover and GPP (Section 5.1). The model is used to predict peatland vegetation dynamics from 1901 to 2020 (Section 5.2).

2. Model Description

2.1. ORCHIDEE-PEAT: Starting Point for New Development

Peatland is represented as an independent soil tile in the model (Figure 1a), its hydrological processes, including rainfall interception, evaporation, transpiration, water infiltration at the soil surface, water diffusion in the soil, and soil surface runoff, are simulated on a half-hourly time step (Qiu et al., 2018). Water infiltration and diffusion in the soil are simulated using an 11-layer scheme (with exponentially increasing layer thickness and totaling 2 m) to solve the Richards diffusion equation. The hydraulic parameters (hydraulic conductivity and diffusivity) for the diffusion equation are calculated using the Mualem-Van Genuchten model (Mualem, 1976; Van Genuchten, 1980). The peatland soil tile is parameterized with peat-specific soil hydraulic properties. More specifically, the peatland soil tile is characterized by a large porosity and high saturated hydraulic conductivity, facilitating a rapid infiltration of rainfall and snowmelt water, and possessing a substantial water storage and retention capacity (Largeron et al., 2018; Qiu et al., 2018). Moreover, if the peatland area fraction within a grid cell is less than 1, the model simulates the hydrological processes typical of fens, which receive precipitation and surface runoff from other biomes within the same grid cell (Qiu et al., 2018). Conversely, if the peatland area fraction is 1, the model simulates the hydrological processes typical of bogs, with precipitation being the only source of water input.

The carbon cycling dynamics of peatland include photosynthetic assimilation, maintenance, and growth respiration of peatland vegetation simulated at a half-hourly timescale, carbon allocation to plant biomass pools, prognostic phenology, and the exchange of carbon between plant biomass pools, litter, and soil carbon pools simulated on a daily basis. For each PFT, there are eight plant biomass pools: leaves, roots, aboveground and belowground sapwood and heartwood, fruits and a plant carbohydrate reserve. Litters are categorized into metabolic and structural carbon pools, both above and below the surface. The three soil carbon pools (active, slow, and passive) are vertically discretized into 32 layers, extending to a maximum depth of 38 m. The decomposition of carbon and carbon flows between the pools are calculated at each layer, controlled by the residence time of carbon in each pool, soil temperature, moisture, and depth. The vertical buildup of peat is parameterized through the downward movement of carbon between soil layers (Qiu et al., 2019).

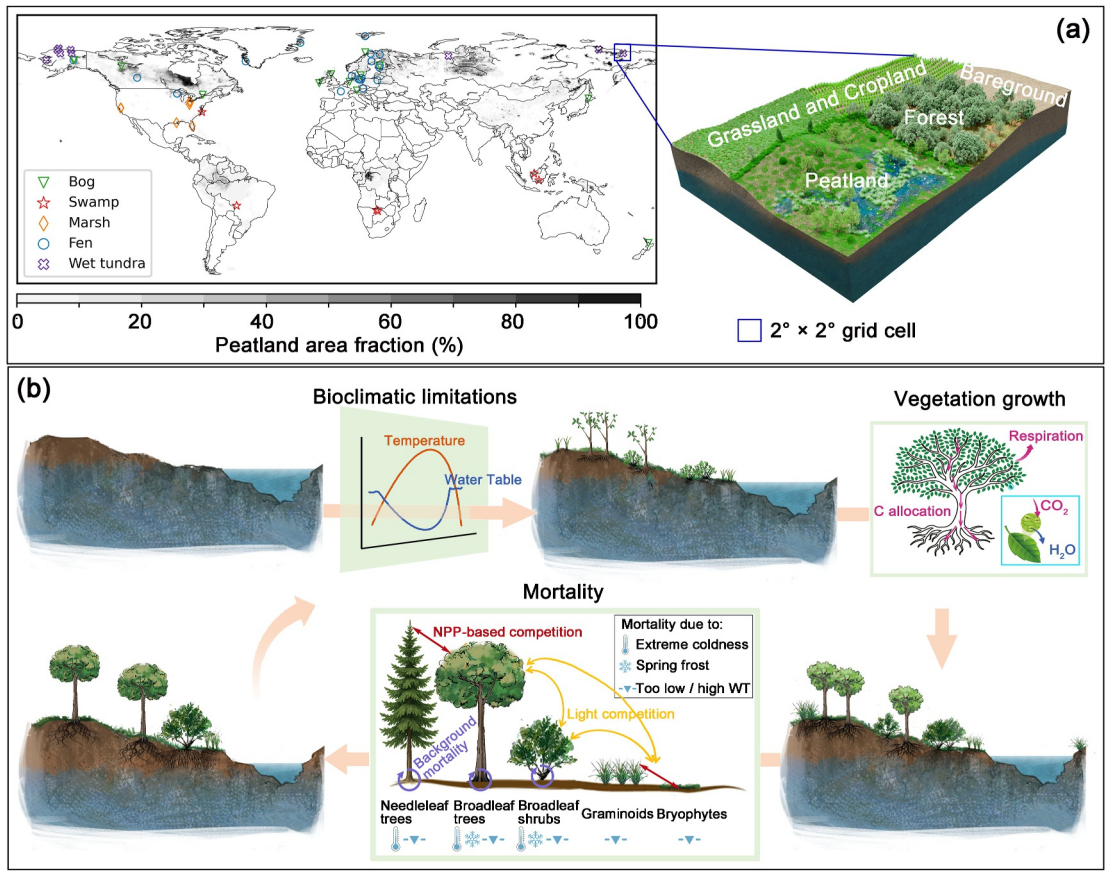

Figure 1. (a) Prescribed distribution of peatlands (the gray map, from Xu et al., 2018), locations of peatland sites used for evaluating the simulated peatland GPP, and representation of four independent soil tiles (one for bare soil, one for all upland trees, one for all upland grasses and crops, and one for peatland) in each model grid cell; (b) a schematic of the peatland vegetation dynamics module. The dynamic area occupied by each peatland PFT is determined by bioclimatic conditions and competition among PFTs. Bioclimatic factors directly constrain the distribution of peatland PFTs (e.g., minimum temperature and water table position required for survival, as shown in Table 1; spring frost and extreme cold can cause tree mortality) and indirectly influence PFT distribution by regulating vegetation growth processes (e.g., photosynthesis and respiration), which subsequently impact the competitive ability of a PFT (e.g., primary productivity and phenological processes influenced by temperature and moisture, such as leaf emergence and senescence).

2.2. Incorporation of New Peatland Plant Functional Types

One characteristic that distinguishes peatlands from upland ecosystems is the presence of specialized vegetation adapted to waterlogged, often acidic and oligotrophic soils. The representation of vegetation in peatlands must take into account (a) the abundant cover of bryophytes, and (b) the development of shallow root systems in plants to avoid oxygen stress beneath the water table (Frolking et al., 2009).

We incorporated a bryophyte PFT as detailed in Druel et al. (2017) into ORCHIDEE-PEAT to represent non-vascular plants such as mosses in peatlands. Considering that bryophytes lack true roots and rely on rhizoids for water acquisition and anchorage, carbon allocation to the root pool is set to be zero in the model. The biomass of bryophytes' non-vascular stems and leaves is represented by the leaf carbon pool in the model and is characterized by "pseudo-stomata" to regulate the exchange of CO_2 and water fluxes with the atmosphere. In comparison to vascular PFTs, the stomatal conductance of the bryophyte PFT is larger but exhibits less sensitivity to humidity and atmospheric CO_2 concentration (Equations 1 and 2 in Druel et al., 2017). While the leaf senescence of the bryophyte PFT is reduced to represent its resistance to extreme conditions, the associated metabolic cost is parameterized as an increase in its leaf biomass carbon turnover (Equation 3 in Druel et al., 2017). Considering that peatland mosses can develop a thick mat under favorable conditions, consequently limiting light and oxygen availability to the lower part of the canopy, the leaf biomass turnover rate of the bryophyte PFT will increase once the maximum LAI is reached (Equation 4 in Druel et al., 2017). During and after drought, peatland moss loses its moisture and dries out (desiccation), resulting in a reduction of its photosynthetic capacity. This process is

Table 1
Bioclimatic Limitations for Peat PFTs

Peat PFT	K_{BG} (yr^{-1})	$T_{min,crit}$ (°C)	T_{grow} (°C)	$WT_{min,crit}$ (m)	$WT_{max,crit}$ (m)	WT_{crit} (m)	k_{WT} (d^{-1})
Bryophytes				0.0	0.5		0.001
C3 graminoids				0.3	0.8		0.0005
BoBS shrubs	0.125	−45	7			0.2	0.001
BoNE trees	0.05	−45	7			0.5	0.001
TrBE trees	0.14	10	7				
TrBR trees	0.14	10	7				

Note. BoBS shrubs: Boreal broadleaf deciduous shrubs; BoNE trees: Boreal needleleaf evergreen trees; TrBE trees: Tropical evergreen trees; TrBR trees: Tropical raingreen trees; K_{BG}: the maximum background mortality rate (Equation 1); $T_{min,crit}$: daily minimum temperature limitation, below which the mortality rate will increase (Equation 2); T_{grow}: mean weekly air temperature during the growing season, below which trees cannot survive; $WT_{min,crit}$, $WT_{max,crit}$, and WT_{crit}: critical WT thresholds used to calculate the mortality of peat PFTs due to WT limitations (Equations 4–6). Positive values of the water table indicate that the water table is below the surface.

accounted for by incorporating a desiccation function to scale the maximum rate of carboxylation and the maintenance respiration of the bryophytes PFT by a monthly running mean hydric stress factor (Equation 6 in Druel et al., 2017), with the hydric stress factor describing the relative water content along the rooting profile.

Vascular plants in peatlands are represented by five PFTs, including a C3 graminoid PFT (Qiu et al., 2018); a boreal needleleaf evergreen tree PFT (Krinner et al., 2005), a tropical evergreen tree PFT (Krinner et al., 2005), a tropical raingreen tree PFT (Krinner et al., 2005), and a boreal deciduous shrub PFT (Druel et al., 2017). All the vascular peat PFTs are parameterized with shallower roots than those in upland ecosystems (Figure S1 in Supporting Information S1).

2.3. Modeling Peatland Vegetation Cover Changes

We revised the vegetation dynamics module of ORCHIDEE-PEAT to distinguish between peatlands and upland ecosystems. All peatland PFTs are assumed to grow exclusively within the peatland soil tile and are thus constrained by the specific conditions of that tile (e.g., peatland water table position). Peatland PFTs thus do not compete with vegetation from upland ecosystems. As such, peatland vegetation dynamics, water and carbon cycles are independently simulated and coupled in the model.

The changes of peatland vegetation cover is simulated on a daily time step by explicitly modeling the introduction and elimination, sapling establishment, light competition and mortality of each PFT. Whether a PFT can be introduced and survive under the prevailing climate conditions is determined by bioclimatic limitations (Figure 1b, Table 1). Plant mortality occurs in response to extreme cold (for woody PFTs), spring frost (for broadleaf woody PFTs), too low/high water table, and competition. In addition, a background mortality is calculated for woody PFTs (Zhu et al., 2015) (Figure 1b).

2.3.1. Background Mortality (M_{BG})

A dynamic background mortality rate, which accounts for the longevity of different woody PFTs and the influence of growth efficiency on mortality, is calculated following Zhu et al. (2015):

$$M_{BG} = \left(\frac{K_{BG}}{1 + 0.035V}\right)/365 \quad (1)$$

where K_{BG} is the maximum background mortality rate (Table 1), proportional to the inverse of the PFT's longevities; V is the growth efficiency of the PFT, defined as the ratio of the net annual biomass increment to the maximum LAI of the preceding year.

2.3.2. Extreme Coldness Induced Mortality (M_{EC})

In the model, woody PFTs are considered adapted to a given climate if the minimum temperature in each day (T_{min}) exceeds a PFT-specific threshold ($T_{min,crit}$) and the mean weekly air temperature during the growing season is greater than 7°C (T_{grow}) (Zhu et al., 2015). If T_{min} falls below $T_{min,crit}$ (extreme coldness, Table 1), the mortality rate increases linearly with decreasing temperature (Zhu et al., 2015):

$$M_{EC} = 0.04 \times (T_{min,crit} - T_{min}), \tag{2}$$

2.3.3. Spring Frost Induced Mortality (M_{SF})

A frost damage limitation is employed to represent the damage caused by spring frost on broadleaf woody PFTs (Zhu et al., 2015). Over the consecutive 40 days after leaf-out, if T_{min} falls below a threshold of −3°C ($T_{SF,crit}$), the tree mortality rate increases with decreasing temperature. Moreover, this mortality rate is multiplied by the time elapsed since leaf-out, as a greater elapsed time implies a larger mass of vulnerable foliage (Zhu et al., 2015):

$$M_{SF}(t, T_{min}) = 0.01 \times (T_{SF,crit} - T_{min}) \left\{ \frac{t - t_{leaf-out}}{40} \right\} \tag{3}$$

Where t is the day of the year; $t_{leaf-out}$ is the day of the year when leaf-out takes place.

2.3.4. Too Low/High Water Table Induced Mortality (M_{WT})

In addition to the temperature-related limitations mentioned above, a critical abiotic factor that impacts the growth of peatland vegetation is water table levels (WT) (Breeuwer et al., 2009). Observational and experimental planting studies have shown that for many peatland grasses and sedges, the survival rate decreases as the WT becomes deeper, and their growth is hindered when the WT is more than 1 m below the surface (Bess et al., 2014; Cooper & MacDonald, 2000; Schipper et al., 2002; Triisberg et al., 2011). In contrast, a shallower water table threshold has been identified as conducive to the growth of peatland moss. For example, to rehabilitate peatland moss in degraded peatlands, the WT is typically raised to around or above the soil surface (Bönsel & Sonneck, 2011; Temmink et al., 2021). We tentatively parameterized a linearly increasing mortality rate for the peatland C3 graminoids PFT and the bryophytes PFT when the mean water table in the preceding month (WT_{month}) falls below $WT_{min,crit}$ but remains above $WT_{max,crit}$ (Table 1, Figure S2 in Supporting Information S1):

$$M_{WT} = k_{WT} \times \mathrm{MIN}\left(1, \mathrm{MAX}\left(0, \frac{WT_{month} - WT_{min,crit}}{WT_{max,crit} - WT_{min,crit}}\right)\right) \tag{4}$$

where k_{WT} is a PFT-specific parameter. WT is diagnosed from the total water volume within the unfrozen soil column as follows:

$$WT = D_{unfrozen} - \sum_{i=1}^{N_{unfrozen}} \frac{(\theta_i - \theta_r)}{(\theta_s - \theta_r)} \Delta z_i \tag{5}$$

where $D_{unfrozen}$ is the total depth of unfrozen soil, $N_{unfrozen}$ is the number of soil layers with temperature above 0℃, Δz_i is the thickness of layer i, θ_i is the volumetric soil moisture of layer i, θ_r, and θ_s are the residual and saturated soil moisture content, respectively. WT is defined as a positive distance below the soil surface, such that increasing WT indicates a lowering of the water table.

While tropical peat swamp trees thrive in waterlogged conditions thanks to their short taproots and extensive root systems, which include lateral roots, aerial roots and split roots, trees in boreal peatlands require WT to be several centimeters to several tens of centimeters below the surface to support their growth (Bussières et al., 2008; Nuyim, 2000). Therefore, for the distribution of the boreal peatland tree PFT and the boreal peatland shrub PFT, the mortality rate increases linearly when WT_{month} is shallower than a PFT-specific critical threshold (WT_{crit}, Table 1):

Table 2
Experimental Design for the Simulations (1850–2021)

Experiment	Atmospheric CO_2 level	Meteorological forcings
Hist	Rising	1901–2021
FixCO2	Fixed at 286 ppm	1901–2021
FixClimate	Rising	Recycled 1901–1920

$$M_{WT} = k_{WT} \times \mathrm{MIN}\left(1, \mathrm{MAX}\left(0, 2 - \frac{WT_{month}}{WT_{crit}}\right)\right) \quad (6)$$

2.3.5. Competition Between Peatland PFTs

In the model, vegetation is represented as a single canopy layer. As such, graminoids and bryophytes do not grow beneath trees/shrubs in the understory, but rather compete with shrubs and trees for space. Light competition between woody vegetation (peatland shrub and tree PFTs) and non-woody vegetation (graminoids and bryophytes PFTs) occurs when the total cover of all peatland PFTs exceeds the prescribed peatland area (Section 3). In such cases, woody vegetation is assumed to receive more light and outcompetes non-woody vegetation, thus the mortality of non-woody PFTs will be increased to reduce their fractional cover. As shrubs are of intermediate height, their area is adjusted when the total cover of peatland woody PFTs exceeds 95% of the prescribed peatland area. Specifically, shrub cover is reduced until the total woody PFT cover no longer exceeds this threshold (Druel et al., 2019). The competition between non-woody PFTs is calculated based on their respective net primary productivity (NPP) such that a more productive PFT is more competitive. The competition between woody PFTs is calculated based on the foliage projective cover of woody PFTs. As the canopy closes and reduces the amount of sunlight, the establishment rate of woody PFTs is reduced (Smith et al., 2001).

3. Simulation Setup

We performed three global simulation experiments at 2° × 2° spatial resolution (Table 2). The Hist experiment is a standard historical simulation, in which the transient period from 1850 to 2021 was forced by historically rising atmospheric CO_2 concentrations and historical meteorological forcing (recycled 1901–1920 meteorological forcing was used for the period 1850–1900 due to the lack of meteorological forcing prior to 1900). To attribute the simulated changes to rising atmospheric CO_2 and climate change, we conducted two additional sensitivity experiments. In the FixCO2 experiment, atmospheric CO_2 concentration was fixed at 286 ppm, while historical meteorological forcing was applied during the transient period. In the FixClimate experiment, atmospheric CO_2 concentration followed historical increases, whereas meteorological forcing was fixed by recycling 1901–1920 conditions throughout the transient period.

Each run was conducted in three steps: (a) The full land surface scheme ORCHIDEE-PEAT was forced for 100 years with repeated 1901–1920 meteorological forcing and constant preindustrial atmospheric CO_2 concentration (286 ppm). (b) The soil carbon sub-model was run for 10,000 years to simulate the accumulation of peat carbon. (c) A transient simulation from 1850 to 2021.

In all three runs, the model was forced by 6-hourly CRU-JRA v2.3 meteorological forcings, which is based on the Japanese Reanalysis data (JRA) (Kobayashi et al., 2015) and adjusted to align with the CRU TS 4.06 data (Harris et al., 2020). The agricultural and forestry use of peatland and net changes of peatland areas were not considered, as the aim of this study is to investigate vegetation shifts within peatlands driven by climate change. Therefore, the area of peatlands (the total coverage of all peatland vegetation types) in each grid cell was fixed and prescribed based on PEATMAP (Xu et al., 2018), with the area of each peatland vegetation types being dynamically simulated as described in Sect. 2 (Figure 1). The area coverage of different upland vegetation types, whose surface runoff is directed to peatlands, was prescribed based on the ESA CCI land cover product (Bontemps et al., 2013) and LUH2v2 data set (Hurtt et al., 2011).

4. Evaluation Data Sets

While peatlands often occur as small-scale, spatially heterogeneous ecosystems, consistent and high-resolution observational data specific to peatlands are very limited. Therefore, model evaluation was largely based on available global data sets. Simulated peatland vegetation distributions were evaluated against ESA WorldCover 2021 data set over global peatland regions as delineated in PEATMAP, a probability map of forested and treed peatlands in Canada, and field survey data on the fraction of grasses, shrubs, mosses and lichens cover at West Siberian wetlands. Simulated peatland GPP was evaluated against three satellite-derived GPP (X-BASE, GOSIF, and VPM) data sets sampled over peatland areas and GPP observations derived from eddy covariance (EC) flux

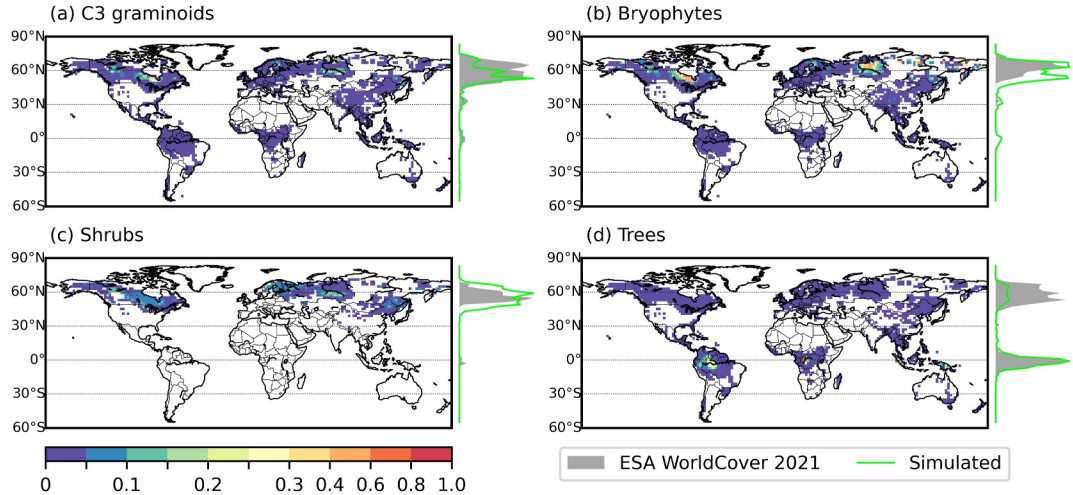

Figure 2. Simulated areal fraction (per unit of total grid cell area) of peatland C3 graminoids (a), bryophytes (b), shrubs (c), and trees (d). The green line and shaded gray area are the normalized latitudinal distribution of simulated and observed (overlay of the ESA WorldCover 2021 product with PEATMAP) peat PFTs, respectively.

towers. Simulated peatland vegetation dynamics (trends in LAI) were evaluated using three satellite LAI (GIMMS LAI4g, GLASS, and GLOBMAP V3) data sets over global peatland regions.

The ESA WorldCover 2021 product was developed and validated using data from Sentinel-1 and Sentinel-2 (Zanaga et al., 2022). It provides global coverage of 11 generic classes at a spatial resolution of 10 m: tree cover, shrubland, grassland, cropland, built-up, bare/sparse vegetation, snow and ice, permanent water bodies, herbaceous wetland, mangrove, moss and lichen, at a resolution of 10 m. To estimate the area of peatland covered by different peat PFTs, we aggregated the ESA WorldCover 2021 land cover data to a resolution of 0.1°, and then performed a pixel-by-pixel overlay of the aggregated data with the 0.1° resolution observation-based peat mask from PEATMAP (Xu et al., 2018). A correspondence table between ESA WorldCover 2021 classes and our peatland PFT is provided in Table S2 in Supporting Information S1.

The probability map of forested and treed peatlands in Canada provides an estimate of the likelihood that a given area has a tree canopy cover greater than 10% and a peat depth greater than 40 cm. Thompson et al. (2016) first used forest structure information (the presence of black spruce or larch, stand height, and stand age) from the Canadian National Forest Inventory, along with bioclimatic variables (mean diurnal range and the standard deviation of monthly temperature), to predict the presence of forested and treed peatlands at the ground plot level. The resulting boosted regression tree model was then applied to predict the distribution of forested and treed peatlands across Canada at a spatial resolution of 250 m.

Simulated peatland vegetation distribution in West Siberia was evaluated against field observations collected from West Siberian wetlands between 1999 and 2013 (Peregon et al., 2008, 2009). A total of 660 field surveys were conducted at 16 sites (Figure 3b), encompassing various wetland types (i.e., fens, bogs) and microtopographical features (i.e., ridges, hollows) at each site. Because the model did not explicitly represent different wetland types or microtopographical variability, site-level averages were used to assess the model performance.

The FLUXCOM-X-BASE (X-BASE for short) GPP product (2001–2021, a spatial resolution of 0.5°) (Nelson et al., 2024) was generated using the FLUXCOM-X framework, which trains machine learning models on in situ EC measurements and applies them globally using a set of predictor variables, including meteorological variables, plant functional type, as well as land surface temperature and vegetation indices from the Moderate Resolution Imaging Spectroradiometer (MODIS). The GOSIF GPP product (2000–2022, a spatial resolution of 0.05°) was produced from OCO-2-based (Orbiting Carbon Observatory-2) SIF (Solar-induced chlorophyll fluorescence) product and linear relationships between SIF and GPP (Li & Xiao, 2019). Eight SIF-GPP relationships with different forms have been used to account for uncertainty from the SIF-GPP relationship. Given that all of the eight SIF-GPP relationships performed well in estimating GPP globally, here we use the ensemble mean to evaluate our model. The vegetation photosynthesis model (VPM) GPP (2000–2016, a spatial resolution of 0.5°)

was estimated from the absorption of light by chlorophyll and the efficiency of converting the absorbed energy to carbon fixed by plants (Zhang et al., 2017). In addition to this improved theory of light use efficiency, a state-of-the-art vegetation index gap-filling and smoothing algorithm and a separate treatment for C3/C4 photosynthesis pathways have been employed. To estimate peatland GPP, we performed a pixel-by-pixel overlay of PEATMAP with the three global GPP data sets mentioned above.

In addition to the three satellite-derived global GPP data sets, 305 site-years of GPP observations from 60 wetland EC sites were used to evaluate the simulated peatland GPP (Figures 1a, Table S1). EC only measures the net exchange of CO_2 (NEE) between the biosphere and atmosphere at the ecosystem level. NEE is then partitioned into GPP and ecosystem respiration (ER) using the nighttime temperature-driven (NT) method (Reichstein et al., 2005) or the daytime temperature-driven (DT) method (Lasslop et al., 2010).

The GIMMS LAI4g LAI product for the years 1982–2015 (a spatial resolution of 1/12°) was generated by biome-specific back propagation neural network models which utilize the latest PKU GIMMS normalized difference vegetation index (NDVI) product and massive high-quality Landsat LAI samples (Cao et al., 2023). Then the GIMMS LAI4g LAI data for the years 2016–2020 was consolidated with the reprocessed Moderate Resolution Imaging Spectroradiometer (MODIS) NDVI product using a pixel-wise fusion method. The GLASS v4 LAI product (1981–2018, a spatial resolution of 0.05°) used in this study was derived from biome-specific general regression neural networks, and is based on the Advanced Very High Resolution Radiometer (AVHRR) surface reflectance data set provided by NASA's long-term data record project (Liang et al., 2021; Xiao et al., 2016). The GLOBMAP v3 LAI product (1982–2020, a spatial resolution of 1/13.75°) was generated by a quantitative fusion of AVHRR LAI (1982–2000) and MODIS LAI (2001–2020) (Liu et al., 2012). MODIS LAI was generated from MODIS surface reflectance data using the GLOBCARBON LAI algorithm, and the LAI for AVHRR was retrieved from GIMMS NDVI.

The ESA WorldCover 2021 product and the satellite-derived GPP and LAI data sets described above were used in their original published form, as provided by the original authors. No reprocessing of the original retrievals or algorithms was performed in this study. For comparison with the model results, these data sets were aggregated to a spatial resolution of 2° × 2° and a monthly temporal resolution. The EC-derived GPP data were obtained from multiple sources. From some sites, GPP was provided directly by site principal investigators, while for others it was obtained from FLUXNET, AmeriFLUX (https://ameriflux.lbl.gov/), and the Integrated Carbon Observation System (ICOS, https://www.icos-cp.eu/) (Table S1). For sites obtained from FLUXNET, AmeriFLUX, and ICOS, we used daytime-partitioned GPP (GPP_DT) because it provides more complete data coverage across sites and years. To assess the sensitivity of our results to the choice of flux partitioning method, we repeated the analysis using nighttime-partitioned GPP (GPP_NT) where available and found that this choice does not affect the main results or conclusions of the study (Figure S3 in Supporting Information S1).

5. Results

5.1. Model Evaluation

By the year 2021, simulated total areas of peatland C3 graminoids, bryophytes, shrubs and trees are 0.6, 1.3, 0.7, and 1.1 million km^2, respectively. Direct and quantitative comparisons between the simulated peatland vegetation cover and the ESA WorldCover 2021 product are challenging, especially in heterogeneous landscapes where multiple vegetation types coexist. The model represents vegetation as a single canopy layer, constraining the sum of vegetation fractions to not exceed 1. In contrast, the ESA WorldCover data set assigns each 10 m × 10 m pixel a single dominant land cover class. For example, a pixel is classified as "tree cover" if trees occupy 10% or more of the area, even if shrubs or herbaceous vegetation are present below the canopy at a higher density than trees. This can lead to overestimation of tree cover and underestimation of shrubs and grasses within the pixel. For instance, high confusion between shrubland and tree classes, as well as between grassland and tree classes, has been reported in the ESA WorldCover 2021 product for Siberian temperate tundra regions (Zanaga et al., 2022). Figures 2a–2c shows that the model broadly captures the latitudinal distribution of bryophytes and shrubs, compared to observations derived by overlaying the ESA WorldCover 2021 product with the PEATMAP peatland distribution map (shaded gray area). However, the model overestimates peatland bryophyte cover in regions between 40°N and 60°N, and underestimates graminoid cover north of 60°N. Compared to the ESA WorldCover data set and the probability map of forested and treed peatlands, boreal peatland tree cover, particularly in the Boreal Plains, Boreal Shield West, and Hudson Plains regions in Canada, appears to be

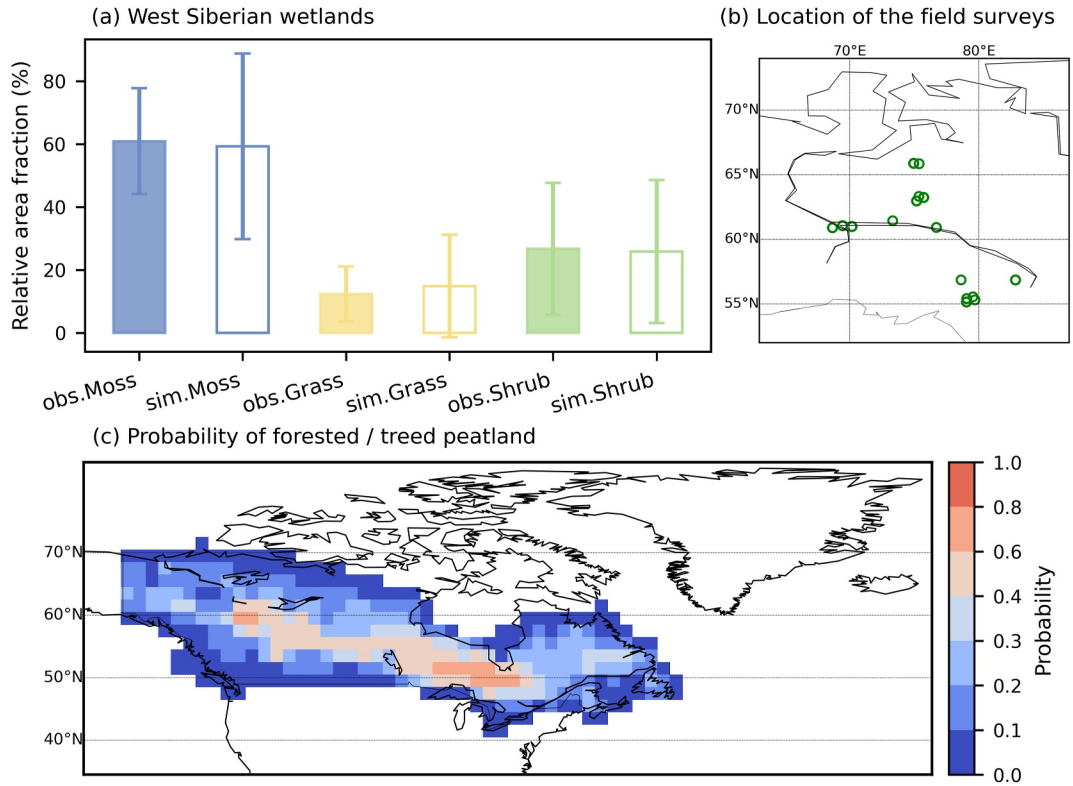

Figure 3. (a) Observed (obs.) and Simulated (sim.) area fraction of peatland bryophytes, graminoids, and shrubs in Western Siberia. (b) The location of the field surveys in Western Siberia. (c) The probability map of forested/treed peatland in Canada (Thompson et al., 2016).

underestimated (Figures 2d and 3c). Note that the probability map indicates the likelihood that each 250 m grid cell has a tree canopy cover greater than 10%. The fundamental differences in how vegetation is represented in the model, the ESA WorldCover data set, and the probability map hinder a more robust evaluation of the model. It is also important to recognize that current estimates of peatland distribution (e.g., PEATMAP) are subject to substantial uncertainties (Hugelius et al., 2020; Xu et al., 2018). Therefore, it is essential to integrate satellite-based observations with ground-based data to enhance the accuracy of peatland mapping and vegetation cover assessments.

We further evaluated the simulated peatland vegetation distribution against field observations from the world's largest high-latitude peatland area, the West Siberian Lowlands (Figures 3a and 3b). In field surveys, graminoids and bryophytes often grow in the understory, which can cause the total vegetation fractions to exceed 1 for a given location. To facilitate comparison between simulated and observed vegetation fractions, we normalized both the observed and simulated fractions of graminoids, bryophytes, and shrubs by their respective totals. Figure 3a shows that the relative coverage of peatland bryophytes, C3 graminoids, and shrubs in the West Siberian Lowlands are well captured by the model.

By overlaying the PEATMAP mask with the three satellite-derived global GPP products, we estimate that global peatland GPP ranges from 4.1 to 5.1 Pg C yr^{-1} for the period 2001–2015 (Figure 4b). Our model predicts higher values, ranging from 5.6 to 6.0 Pg C yr^{-1} over the same period. In temperate and boreal regions (north of 23.5°N), the simulated peatland GPP (averaged over the period 2001–2015) exceeds all three satellite-derived estimates by 0.7 (X-BASE) to 1.0 (VPM) Pg C yr^{-1} (Figures 4c–4f). In tropical regions (south of 23.5°N), the simulated peatland GPP closely matches the GOSIF estimate, with a difference of less than 0.01 Pg C yr^{-1}, while it is higher than the X-BASE and VPM estimates by 0.4 and 0.6 Pg C yr^{-1}, respectively. The model captures the pronounced seasonal cycle of GPP in temperate and boreal peatlands, but it overestimates peak values during the growing season (Figure 5a). In tropical peatlands, the model simulates weaker seasonality and smaller interannual

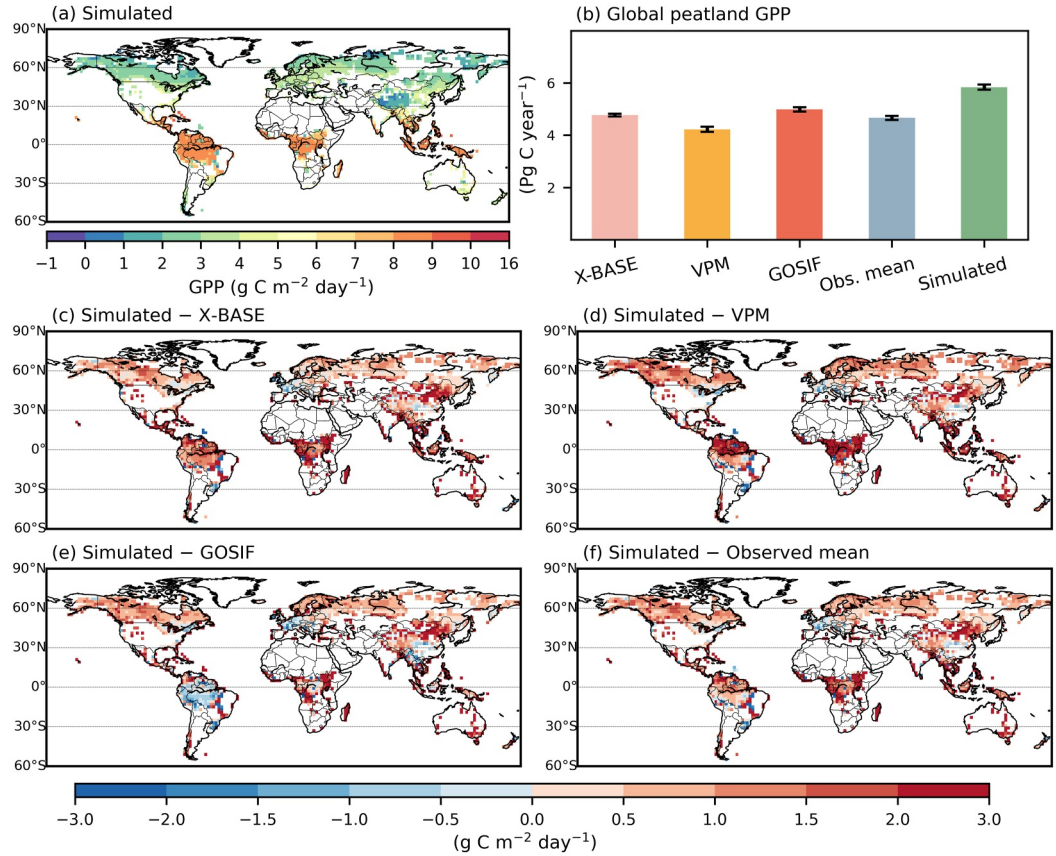

Figure 4. Simulated peatland GPP averaged over 2001–2015 (a); global total peatland GPP from the three satellite-derived data sets (X-BASE, VPM, GOSIF), their average, and the model simulation (b); differences between the model and satellite-derived estimates from X-BASE(c), VPM (d), and GOSIF (e), and their average (f).

variability compared to satellite-derived GPP products, and consistently overestimates GPP throughout the entire period (Figure 5b).

It is worth acknowledging that satellite-derived global GPP products provide aggregated GPP values that account for all ecosystems within each grid cell, which may include a diverse range of land cover types beyond just peatlands. Therefore, the estimated peatland GPP from global satellite GPP products may be subject to uncertainties due to potential mismatches between peatland-specific GPP and the general ecosystem GPP values reported by these products, as well as variations in methodology and spatial resolution across different data sets. In addition, by reconciling GPP estimates with soil respiration data, a recent study inferred a global GPP that is approximately 32% higher than estimates derived from satellite remote sensing products or satellite-driven upscaling approaches (Jian et al., 2022). Therefore, the apparent positive bias in simulated GPP relative to satellite-derived estimates does not necessarily imply an overestimation of peatland GPP by the model. To further assess model performance using an independent observational constraint, we compared simulated GPP with observations from peatland eddy covariance sites (305 site-years from 60 wetland sites). This comparison indicates that the model slightly overestimates peatland GPP, with a mean bias error of 0.61 g C m^{-2} day^{-1} (Figure 6).

Figure 7 presents trends in LAI from 1982 to 2018, derived from three remote sensing data sets and the model simulation (values reported below are in m^2 m^{-2} yr^{-1}). The model reproduces the observed LAI trend of global peatlands from 1982 to 2012 well, with a simulated rate of change of 0.002 (Figure 7f). In comparison, the observed LAI trends from the three remote sensing data sets range from 0.001 (GIMMS) to 0.003 (GLOBMAP), with an average trend of 0.002. However, while the observed LAI trends from 2012 to 2018 range from −0.002 (GLASS) to 0.007 (GLOBMAP), the simulated LAI trend is −0.004. Thus, the model underestimates the rate of LAI change of global peatlands during this period. Similar to the satellite-derived GPP products, these remote

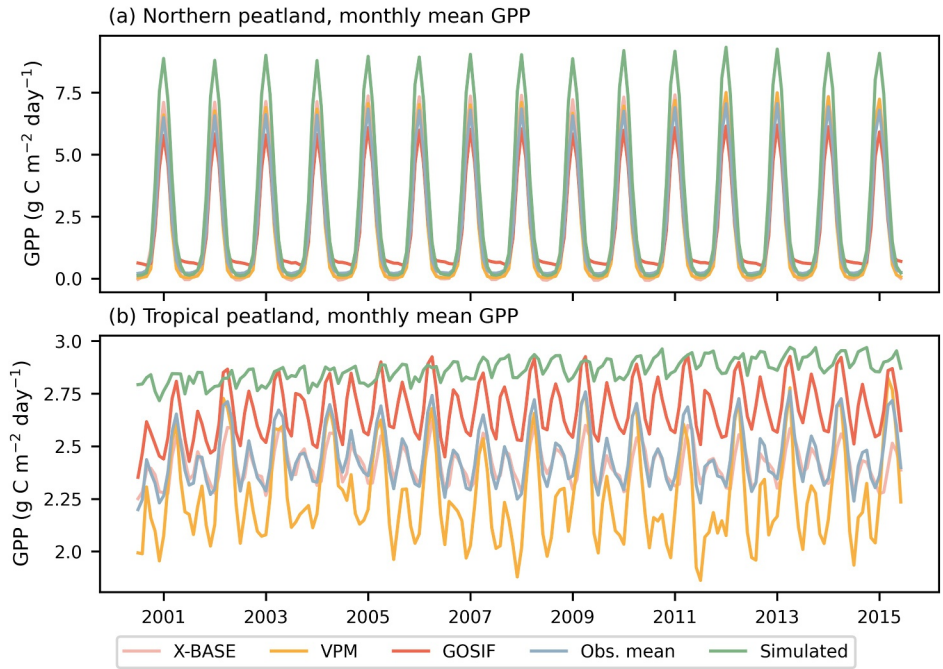

Figure 5. Simulated and observed monthly GPP for northern peatlands (north of 23.5°N) (a) and tropical peatlands (south of 23.5°N) (b).

sensing LAI data sets are not specific to peatlands. They are better suited for evaluating simulated LAI in regions where peatlands are more prevalent, such as the Hudson Bay Lowlands (HBL), the West Siberian Lowlands (WSL), and the central Congo Basin. For these three peatland complexes, The GIMMS data set exhibits the smallest LAI change from 1982 to 2018 (10^{-5}, 10^{-4} and 10^{-5} for HBL, WSL, and the Congo Basin, respectively), while the GLOBMAP data set shows the largest increase in LAI (0.001, 0.0004 and 0.0004 for HBL, WSL, and the Congo Basin, respectively). The simulated peatland LAI trend falls within the range of these observations (10^{-5}, 0.0002 and 10^{-5} for HBL, WSL, and the Congo Basin, respectively).

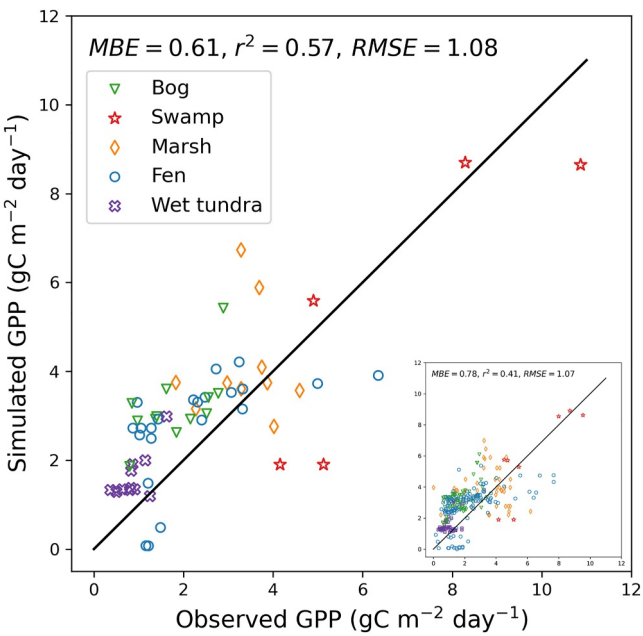

Figure 6. Observed (x axis) and simulated (y axis) GPP (multi-year mean) at 60 wetland sites (Figure 1a, Table S1). The inset shows observed and simulated GPP across individual 305 site-years. MBE: mean bias error; RMSE: root mean square deviation; r^2: coefficient of determination.

5.2. Peatland Vegetation Dynamics Over the Last Century

From 1901 to 2020, the model predicts an increase in the water table depth across northern peatlands (Figure S4 in Supporting Information S1). As a result of this deeper water table and hence drier growing conditions, the areas covered by peatland bryophytes and C3 graminoids in northern regions are simulated to decrease by 0.2 million km^2 (13%) and 0.1 million km^2 (13%), respectively, while the coverage of peatland shrubs and peatland trees is predicted to increase by 0.3 million km^2 (75%) and 0.03 million km^2 (2%), respectively (Figures 8 and 9a). In addition to drier conditions, climate warming may also contribute to shrub and tree expansion by reducing cold-related mortalities (Zhu et al., 2015). The shift in peatland vegetation is most pronounced in the Northwest Territories of Canada, Western Canada, and the Russian Far East. In the two major northern peatland complexes, HBL and WSL, changes in vegetation cover are relatively small in absolute terms but substantial in percentage terms (Figures 9b and 9c). In the HBL, non-woody plants decline by 0.02 million km^2 (6%), while shrubs expand by 0.03 million km^2 (105%). In the WSL, non-woody plants decrease by 0.05 million km^2 (11%), while shrubs expand by 0.04 million km^2 (62%). Tree expansion in the HBL is negligible, while in the WSL, it increases by 0.01 million km^2 (27%). The water table and air temperature (Figure S5 in

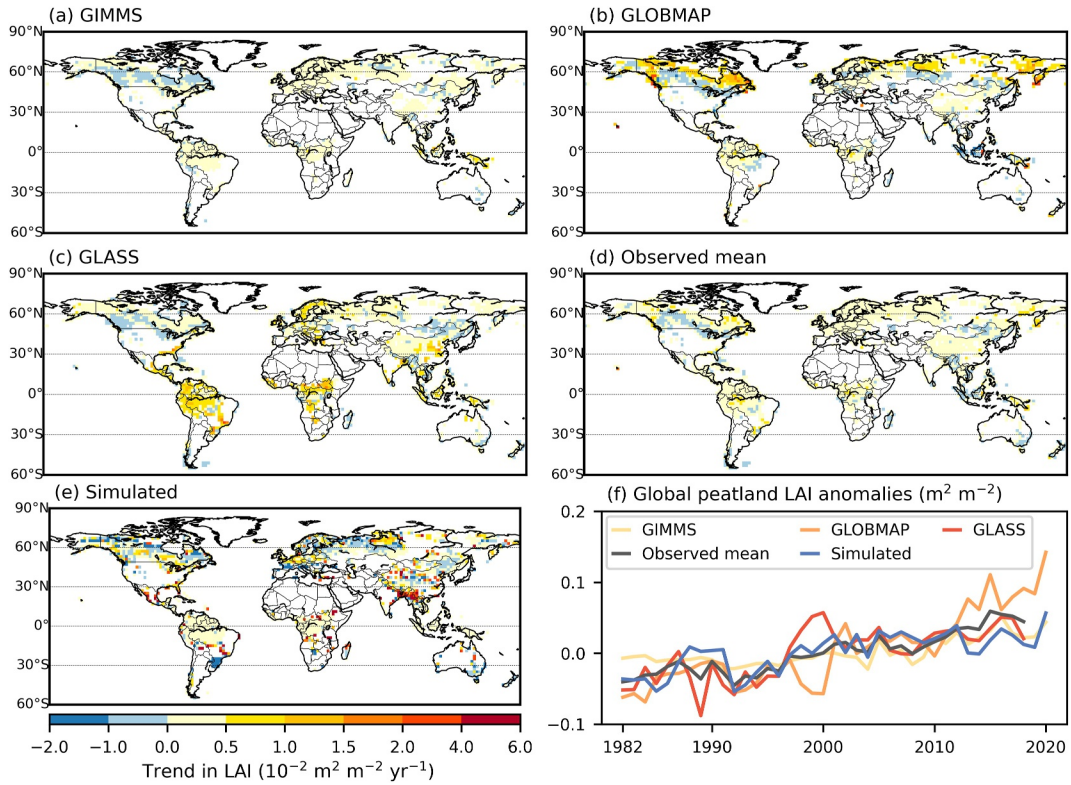

Figure 7. Trend in LAI from 1982 to 2018 from the GIMMS (a), GLOBMAP (b), and GLASS (c) data sets, their average (d), and trend in the simulated peatland LAI (e). Panel (f) presents the anomaly of global peatlands LAI.

Supporting Information S1) of tropical peatlands remained relatively stable, leading to negligible changes in the vegetation composition.

We conducted two additional simulations (FixCO2 and FixClimate, Table 2) to study the impact of the two primary drivers, rising atmospheric CO_2 and climate change, on the simulated distribution of peatland vegetation. In response to rising atmospheric CO_2 levels, plants enhance their assimilation rate and improve water use efficiency. The resulting increase in photosynthetic capacity and NPP of trees leads to greater coverage of trees (Zhu et al., 2015). When the atmospheric CO_2 is held constant at 286 ppm (FixCO2), the model predicts an expansion of peatland shrubs and trees by 0.14 million km^2, from 1901 to 2020. This increase is only 45% of that predicted in the Hist simulation (Figure 10). Trees and shrubs have a competitive advantage over graminoids and bryophytes because of their superior access to light. Additionally, their expansion increases transpiration, leading to drier conditions that are unfavorable for bryophytes and graminoids. Therefore, the smaller expansion of trees and shrubs in the FixCO2 simulation alleviates pressure on graminoids and bryophytes. Consequently, the decline in bryophytes and C3 graminoids area in the FixCO2 simulation is 0.16 million km^2 smaller than in the Hist simulation. In the FixClimate simulation, repeated 1901–1920 meteorological forcing is used to drive the model. Compared to the Hist simulation, the FixClimate simulation predicts wetter and cooler peatland conditions in Alaska, northern Canada, Central and Southern Europe, and the Russian Far East, which restrict the expansion of peatland shrubs and trees (Figures S5 and S6 in Supporting Information S1). As a result, shrub and tree cover increases by only 0.03 million km^2 in FixClimate simulation, which is only 10% of that predicted in the Hist simulation. These results suggest a synergistic interaction between rising atmospheric CO_2 and climate change, where their combined impact drives greater tree and shrub expansion than what would be expected from their individual effects alone.

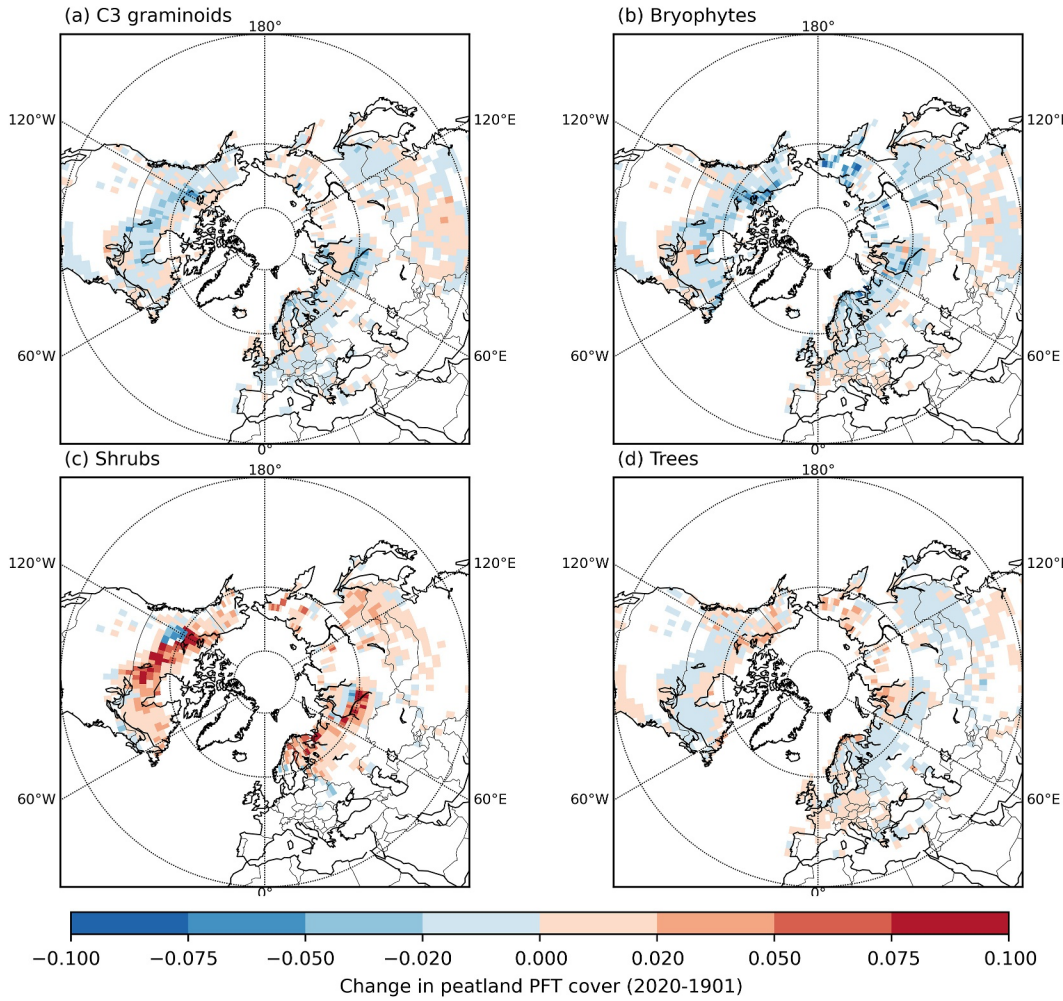

Figure 8. Simulated change (2020–1901) in the fractional cover of peatland C3 graminoids (a), peatland bryophytes (b), peatland shrubs (c), peatland trees (d).

6. Discussion

6.1. Peatland Modeling and Evaluation Challenges

A critical challenge in peatland modeling is the difficulty in constraining key parameters and process representations (Hou et al., 2023). In this study, we improved ORCHIDEE-PEAT by incorporating multiple peatland-specific PFTs into a dedicated peatland soil tile and simulating dynamic competition among these PFTs. While the original single-PFT model substantially underestimates global peatland GPP, the new model simulates greater GPP values that are closer to the satellite-based estimates, though it exhibits a positive bias (Figure S7a in Supporting Information S1). Both the original single-PFT model and the new model capture the overall increasing trend in peatland LAI since the early 1980s (Figure S7b in Supporting Information S1). However, the new model simulates greater interannual variability in LAI. These results indicate that a more detailed representation of peatland vegetation and interactions among different vegetation types, as implemented in the new model, can substantially affect the magnitude and variability of simulated peatland vegetation structure and productivity.

The positive bias in simulated peatland GPP likely reflects uncertainties in the parameterization of peatland PFTs in the new model, including key parameters (e.g., photosynthetic capacity and rooting depth), as well as the functional relationships describing vegetation responses to environmental drivers (e.g., mortality in response to water table depth and its variability), which are currently based on simplified assumptions or broad generalizations. In the absence of observational or experimental constraints, a comprehensive sensitivity analysis in future studies could help guide further refinement of these parameterizations.

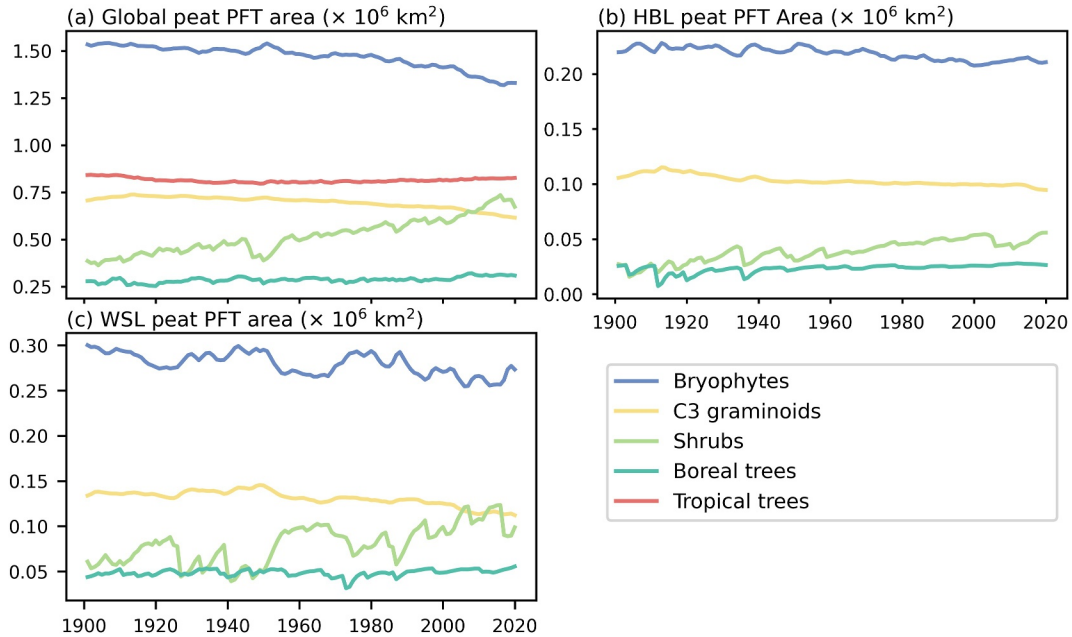

Figure 9. Historical change in the area of peat vegetation in the Hist run for the global domain (a), the HBL region (b), and the WSL region (c).

While the performance of ORCHIDEE-PEAT in the evaluation is encouraging, evaluation is complicated by the scarcity of spatially and temporally consistent observational data specific to peatlands. Existing remote sensing products, such as global GPP and LAI data sets, include limited training data from peatland flux tower sites and are therefore not specifically calibrated for peatland ecosystems. They are influenced by mixed land cover types within each pixel. Ground-based data sets, while more reliable, remain geographically sparse and often lack co-located measurements of carbon fluxes and vegetation structure. Furthermore, uncertainties in peatland extent, as seen in global maps like PEATMAP, propagate into both model forcing and evaluation metrics. To benchmark models, it is crucial to obtain:

1. Peatland distribution and vegetation composition: The hidden nature of peat layers beneath the surface makes it difficult to distinguish between peatland and non-peatland areas. In addition, peatlands are often small and interspersed with non-peatland ecosystems. To address these challenges, a combination of advanced remote sensing data and multi-source data is essential for creating a high-resolution map of peatland distribution and vegetation covers (Karlson & Bastviken, 2023). Moreover, reconstructing historical peatland distribution and vegetation changes remains a critical gap that needs to be addressed.
2. Peatland vegetation and C fluxes measurement: Despite growing recognition of the crucial role of peatlands in carbon storage and climate regulation, observational constraints on peatland vegetation dynamics and carbon

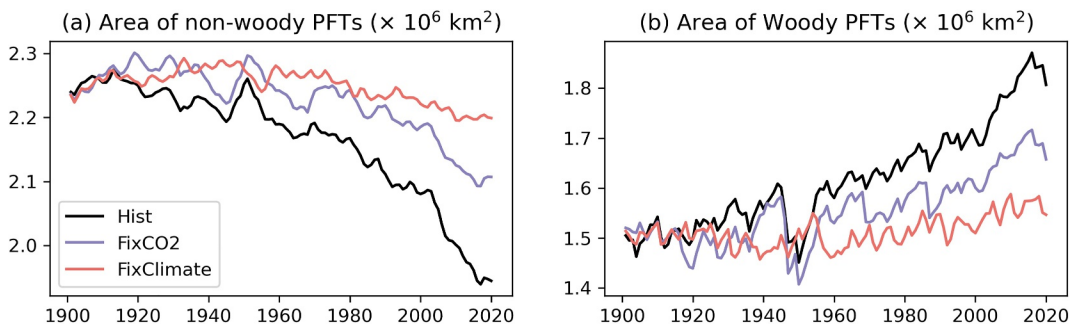

Figure 10. Evolution of global area of peatland non-woody plants (bryophytes and C3 graminoids) (a), and woody plants (shrubs and trees (b) from 1901 to 2020 in the Hist, FixCO2 and FixClimate experiments.

fluxes remain limited and unevenly distributed across regions (Zhao et al., 2024). Although recent efforts have expanded peatland and wetland observation databases, these data sets remain biased toward boreal and Arctic regions, with tropical peatlands largely underrepresented (Olefeldt et al., 2021; Peltola et al., 2019; Virkkala et al., 2022). Moreover, substantial uncertainties persist in the spatial upscaling of ecosystem CO_2 fluxes due to limited site coverage and strong environmental heterogeneity (Virkkala et al., 2021). Therefore, Expanded monitoring networks and improved sampling methodologies are essential for obtaining more accurate and representative estimates of peatland vegetation dynamics and C fluxes (López-Blanco et al., 2024).

6.2. Vegetation Shifts in Northern Peatlands

The model predicts a shift in vegetation composition in northern peatlands from 1901 to 2020, characterized by a decline in non-woody PFTs and an expansion of woody PFTs. This aligns with field observations of shrubification and woody encroachment in northern peatlands (McPartland et al., 2020; Norby et al., 2019). Changes in vegetation composition can significantly influence peatland carbon cycling. For example, an expansion of graminoids could increase CH_4 emission rates, as the aerenchyma tissue of graminoids facilitates the transport of CH_4 from the anoxic zone of the soil directly to the atmosphere, bypassing the aerobic zone where CH_4 oxidation takes place (Goud et al., 2017). An expansion of shrubs could enhance peatland C uptake by increasing ecosystem productivity (Ratcliffe et al., 2019). However, its impact on peatland net ecosystem exchange remains uncertain, as field studies have reported conflicting results. In some cases, the expansion of shrubs can decrease ecosystem respiration, due to modification of the microbial community and the build-up of phenolics (Wang et al., 2015, 2021). In other cases, the expansion of shrubs can promote the respiration of ancient peatland carbon due to priming effects (Gavazov et al., 2018; Walker et al., 2016).

Previous modeling studies have shown that the long-term effects of climate change on peatland carbon storage are modulated by shifts in vegetation composition. Sulman et al. (2013) showed that in a small, wetland-rich landscape in northern Wisconsin, USA, a declining water table can lead to an expansion of wet-tolerant woody species and dry upland communities, thereby increasing biomass carbon. Their study also highlighted that the relative importance of plant community changes and peatland soil decomposition for the peatland carbon balance can vary substantially depending on the timescale considered and the magnitude of water table decline. Heijmans et al. (2008) examined the long-term impacts of climate change on vegetation and carbon dynamics in two northern bogs, and found that the effects of warming can be compensated by increases in atmospheric CO_2 and precipitation. While quantifying the effects of vegetation change on peatland C balance is beyond the scope of this study, the model presented here integrates dynamic peatland vegetation with peatland-specific hydrology and carbon cycling, thus is a useful tool for assessing large-scale, vegetation mediated climate change impacts on peatland carbon dynamics in future applications.

6.3. Limitations of the Model and Future Development Needs

The current version of the model includes established mechanistic processes related to peatland vegetation, carbon dynamics and hydrology. Nevertheless, nutrient competition among vegetation types is not considered due to the absence of a nutrient cycle in the model. Another limitation is the simplified representation of peatlands as homogenous within each grid cell, without distinguishing between different peatland types within the coarse $2° \times 2°$ grid. Fens and bogs are the two main types of peatlands, and they differ in their hydrology, soil pH, nutrient availability, and vegetation composition. Bogs receive water and nutrients only from atmospheric sources, which leads to nutrient-poor and acidic conditions that favor *Sphagnum* mosses and support some woody shrubs. In contrast, fens are fed not only by atmospheric precipitation, but also by groundwater and surface water inputs. As a result, fens are typically (though not always) wetter and richer in nutrients, have higher soil pH than bogs, and harbor a greater abundance of graminoids and brown moss species (Graham et al., 2016; Griffiths et al., 2019). In the current model configuration, peatlands receive surface runoff from other biomes within the same grid cell. The larger the peatland fraction in a grid cell, the smaller the lateral runoff input from other soil tiles to the peatland. Therefore, peatlands in the model effectively span a continuum between fen-like and bog-like hydrological conditions. However, at the coarse spatial resolution of this study, no grid cell is entirely covered by peatland, and therefore no peatlands can be classified as pure bogs. In a sensitivity experiment in which lateral surface runoff inputs from non-peatland biomes to peatlands were suppressed, the model simulates a lower water table, leading to reduced coverage of C3 graminoids and bryophytes and increased coverage of shrubs and trees (Figure S8 in Supporting Information S1). While fen-bog hydrological differences in the model affect the

magnitude of peatland PFT area fractions, the trends in global peatland vegetation dynamics reported in this study remain unchanged (Figure S8 in Supporting Information S1). Yet, a more explicit sub-grid representation of fens and bogs could be important for capturing spatial heterogeneity in vegetation composition within peatland complexes, as well as peatland responses to warming and drying (Graham et al., 2016; Weltzin et al., 2000).

As in most land surface models, ORCHIDEE-PEAT represents vegetation using a single-layer canopy. As a result, light competition among trees, as well as the shading effects of trees on understory vegetation are implicitly represented rather than explicitly simulated. This simplification may affect the realism of vegetation competition and coexistence, particularly at local scales where vertical canopy structure and light gradients play an important role. In addition to light-mediated interactions, peatland vegetation dynamics are also influenced by other biotic interactions that are not explicitly represented in the current model. For example, mosses can inhibit the germination, growth and establishment of vascular plants through allelopathic effects (Whitehead et al., 2018). In addition, thick and dense moss cushions can prevent seeds from reaching the soil and alter the light and nutrient regime for seedlings (Turetsky et al., 2012). These processes can strongly regulate plant recruitment and vegetation competition in peatlands, thus represent an important direction for future model development.

Fire is an important disturbance that shapes ecosystem vegetation composition and structure (Dickson-Hoyle et al., 2024). Fire can eliminate dominant species, allowing less competitive or fire-adapted species to establish and thrive (Guêné-Nanchen et al., 2022; Shepherd et al., 2021). Additionally, fire can alter soil properties and hydrology, thus indirectly affecting post-fire peatland vegetation recovery (Jones et al., 2022). The fire module in the model (Yue et al., 2014, 2015) was not activated in this study, as it requires further refinement to accurately account for peatland-specific conditions, such as water table fluctuations, peat depth variability, and its unique smouldering fire characteristics. Human land management and land use change represent another major disturbance that alters peatland vegetation dynamics. While these changes are detectable in remote sensing observations, they are not accounted for in this study. As a result, they contribute to uncertainties when comparing simulated and observed vegetation dynamics, and should be considered in future studies (Leifeld & Menichetti, 2018; Qiu et al., 2021).

Our simulations reveal a long-term change in northern peatland PFTs, with a decline in bryophytes and C3 graminoids and an expansion of shrubs and trees since 1901. While this indicates a taxonomic shift at the level of broad functional groups, it remains uncertain whether such changes reflect functional changes at the ecosystem level. A previous study has shown that taxonomic and functional turnover are decoupled in European peat bogs (Robroek et al., 2017). Our model does not explicitly represent species-level processes or within-PFT trait variability. Future developments could incorporate trait-based representations of PFTs or allow for intra-PFT diversity to better capture the diverse response of peatland vegetation species to climate change, and to assess functional resilience of peatland ecosystems in response to species turnover.

7. Conclusions

Peatlands have increasingly been incorporated into land surface models (LSMs) since the 2010s (Chaudhary et al., 2017; Kleinen et al., 2012; Spahni et al., 2013; Stocker et al., 2014; Wania et al., 2009). As the peatland modeling framework advances rapidly, there is a growing need to enhance our understanding of peatland vegetation dynamics and its interactions with hydrological and carbon cycling processes (Qiu et al., 2022). The ORCHIDEE-PEAT model presented here incorporates peatland-specific vegetation and integrates peatland vegetation dynamics with hydrological and carbon cycling processes. These improvements are crucial for accurately predicting the impact of climate change on peatlands and understanding how peatlands feedback into climate change.

Model evaluation against multiple independent data sets shows that ORCHIDEE-PEAT is able to capture the large-scale distribution of peatland vegetation types and the long-term trends in peatland LAI, but it exhibits a positive bias in simulated peatland GPP. Applying the model to historical climate conditions reveals large-scale shifts in peatland vegetation composition over the twentieth century, characterized by declines in bryophyte and C3 graminoid cover and an expansion of boreal shrubs and trees. While increased shrub and tree productivity may enhance carbon uptake, associated increases in ecosystem respiration and changes in hydrological conditions could offset or even reverse this effect. The model provides a framework for investigating how climate change may alter peatland vegetation structure and carbon balance in future studies.

Acknowledgments
This work was supported by the National Key R&D Program of China (2022YFF0802104) and the National Natural Science Foundation of China (32430065). P.C., L.L, A.L., M.K. and A. K. acknowledge support from the European Union's Horizon Europe programme WET HORIZONS, grant agreement no. 101056848. P.C. acknowledge support from the CALIPSO (Carbon Loss in Plant Soils and Oceans) project, funded through the generosity of Eric and Wendy Schmidt by recommendation of the Schmidt Futures program. B.G. and A.M.P acknowledge support from the European Union's H2020 HoliSoils (H2020 grant agreement 101000289). D.Z. acknowledge support from the National Natural Science Foundation of China (42571104). The work of N.P.K. and N.P.M.–T. was carried out according to the state order of the Institute of Soil Science and Agrochemistry SB RAS, with the financial support of the Ministry of Science and Higher Education of the Russian Federation. E.L.B, considers this study a contribution to GreenFeedBack (Greenhouse gas fluxes and earth system feedbacks) funded by the European Union's HORIZON research and innovation program under grant agreement No 101056921. J.D. acknowledges support from Research infrastructure projects of the Ministry of Education, Youth and Sports of the Czech Republic LM2023048. E.E. and C.E. acknowledge support from The National Science Foundation Grants DEB LTREB 1354370 and 2011257, DEB-0425328, DEB-0724514, DEB-0830997, and the US Geological Survey Climate R&D program. K.F. and W.P. acknowledge support from the National Science Centre, Poland under project UMO-2020/37/B/ST10/01219. A. L. and M. K. acknowledge the Ministry of Transport and Communications through the Integrated Carbon Observing System (ICOS) research and ICOS Finland. M.P. and K.D.N. acknowledge funding from the Swedish Research Council (VR, Grants 2018-03966, 2019-04676) and the Kempe Foundation (Grants JCK-1712, JCSMK23-0221), as well as the financial support from VR and contributing research institutes to the Swedish Infrastructure for Ecosystem Science (SITES) and the Swedish Integrated Carbon Observation System (ICOS-Sweden). FLUXNET data products were produced and harmonized by eddy covariance regional networks and data processing centers, including AmeriFlux, ChinaFlux, European Fluxes Database, ICOS, JapanFlux, KoFlux, OzFlux, SAEON, and TERN. We would like to thank the FLUXNET team, ICOS Ecosystem Thematic Centre, and the AmeriFlux program for processing and harmonizing the data. Funding for the AmeriFlux data service was provided by the U.S. Department of Energy Office of

Conflict of Interest

The authors declare no conflicts of interest relevant to this study.

Availability Statement

The FLUXNET2015 data set (FLUXNET, 2015) and AmeriFlux data (AmeriFlux, 2024) were obtained from FLUXNET data portal (https://fluxnet.org/data/download-data/) and AmeriFlux data portal (https://ameriflux.lbl.gov/data/download-data/). The Warm Winter 2020 ecosystem eddy covariance flux product was downloaded from the ICOS Carbon portal (https://www.icos-cp.eu/data-products/2G60-ZHAK), with DOI: https://doi.org/10.18160/2G60-ZHAK (Warm Winter 2020 Team et al., 2022). The DOIs for the AmeriFlux sites used in this study include the following: https://doi.org/10.17190/AMF/1881563 (Vourlitis et al., 2025), https://doi.org/10.17190/AMF/1562387 (Hinkle & Bracho, 2019), https://doi.org/10.17190/AMF/1543387 (Ward et al., 2025), https://doi.org/10.17190/AMF/1871144 (Shortt et al., 2025), https://doi.org/10.17190/AMF/1871139 (Matthes et al., 2022), https://doi.org/10.17190/AMF/2204881 (Eichelmann et al., 2025), https://doi.org/10.17190/AMF/1881595 (Valach, Kasak, et al., 2025), https://doi.org/10.17190/AMF/1832165 (Valach, Shortt, et al., 2025), https://doi.org/10.17190/AMF/1832164 (Bohrer, 2025), https://doi.org/10.17190/AMF/1871142 (Bohrer & McMurray, 2022), https://doi.org/10.17190/AMF/2229402 (Chen & Chu, 2025), https://doi.org/10.17190/AMF/2448423 (Humphreys & Lafleur, 2024), https://doi.org/10.17190/AMF/1246071 (Desai, 2025), https://doi.org/10.17190/AMF/1436323 (Flanagan, 2018), https://doi.org/10.17190/AMF/2469439 (Sonnentag & Quinton, 2025), https://doi.org/10.17190/AMF/1881569 (Euskirchen, 2025a), https://doi.org/10.17190/AMF/1881570 (Euskirchen, 2025b), https://doi.org/10.17190/AMF/1902838 (Torn & Dengel, 2025a), https://doi.org/10.17190/AMF/1480322 (Ueyama et al., 2025), https://doi.org/10.17190/AMF/1246067 (Zona & Oechel, 2019), https://doi.org/10.17190/AMF/1871138 (Euskirchen et al., 2025), https://doi.org/10.17190/AMF/1246029 (Zona & Oechel, 2016), https://doi.org/10.17190/AMF/1832162 (Torn & Dengel, 2025b), https://doi.org/10.17190/AMF/1498753 (Sullivan et al., 2025). The full list of sites, including site locations, data set DOIs, and corresponding citations, is provided in Table S1.

The ORCHIDEE-PEAT model (Qiu, 2026a) codes used in this study is open-source and available at https://doi.org/10.5281/zenodo.18241888 Model outputs (Qiu, 2026b) presented in this study are available at https://doi.org/10.5281/zenodo.18382534.

References

AmeriFlux. (2024). AmeriFlux BASE data products [Dataset]. *Lawrence Berkeley National Laboratory*. Retrieved from https://ameriflux.lbl.gov/data/download-data/

Belyea, L. R., & Baird, A. J. (2006). Beyond "the limits to peat bog growth": Cross-scale feedback in peatland development. *Ecological Monographs*, *76*(3), 299–322. https://doi.org/10.1890/0012-9615(2006)076[0299:BTLTPB]2.0.CO;2

Bess, J. A., Chimner, R. A., & Kangas, L. C. (2014). Ditch restoration in a large northern Michigan fen: Vegetation response and basic porewater chemistry. *Ecological Restoration*, *32*(3), 260–274. https://doi.org/10.3368/er.32.3.260

Bjorkman, A. D., García Criado, M., Myers-Smith, I. H., Ravolainen, V., Jónsdóttir, I. S., Westergaard, K. B., et al. (2020). Status and trends in Arctic vegetation: Evidence from experimental warming and long-term monitoring. *Ambio*, *49*(3), 678–692. https://doi.org/10.1007/s13280-019-01161-6

Bjorkman, A. D., Myers-Smith, I. H., Elmendorf, S. C., Normand, S., Rüger, N., Beck, P. S. A., et al. (2018). Plant functional trait change across a warming tundra biome. *Nature*, *562*(7725), 57–62. https://doi.org/10.1038/s41586-018-0563-7

Bohrer, G. (2025). AmeriFlux FLUXNET-1F US-ORv Olentangy River Wetland Research Park (version 5–7) [Dataset]. *AmeriFlux AMP*. https://doi.org/10.17190/AMF/1832164

Bohrer, G., & McMurray, S. E. (2022). AmeriFlux FLUXNET-1F US-OWC old woman creek (version 3–5) [Dataset]. *AmeriFlux AMP*. https://doi.org/10.17190/AMF/1871142

Bönsel, A., & Sonneck, A.-G. (2011). Effects of a hydrological protection zone on the restoration of a raised bog: A case study from Northeast-Germany 1997–2008. *Wetlands Ecology and Management*, *19*(2), 183–194. https://doi.org/10.1007/s11273-011-9210-x

Bontemps, S., Defourny, P., Radoux, J., Van Bogaert, E., Lamarche, C., Achard, F., et al. (2013). Consistent global land cover maps for climate modelling communities: Current achievements of the ESA' land cover CCI. In *Presented at the ESA Living Planet Symposium* (Vol. 722, p. 62). Retrieved from https://ui.adsabs.harvard.edu/abs/2013ESASP.722E..62B

Bragazza, L., Parisod, J., Buttler, A., & Bardgett, R. D. (2013). Biogeochemical plant–soil microbe feedback in response to climate warming in peatlands. *Nature Climate Change*, *3*(3), 273–277. https://doi.org/10.1038/nclimate1781

Breeuwer, A., Robroek, B. J. M., Limpens, J., Heijmans, M. M. P. D., Schouten, M. G. C., & Berendse, F. (2009). Decreased summer water table depth affects peatland vegetation. *Basic and Applied Ecology*, *10*(4), 330–339. https://doi.org/10.1016/j.baae.2008.05.005

Bussières, J., Boudreau, S., & Rochefort, L. (2008). Establishing trees on cut-over peatlands in eastern Canada. *Mires Peat*, *3*(10), 1–12. https://doi.org/10.19189/001c.128263

Cao, S., Li, M., Zhu, Z., Wang, Z., Zha, J., Zhao, W., et al. (2023). Spatiotemporally consistent global dataset of the GIMMS leaf area index (GIMMS LAI4g) from 1982 to 2020. *Earth System Science Data*, *15*(11), 4877–4899. https://doi.org/10.5194/essd-15-4877-2023

Science. We thank Rebekka Artz for her constructive comments on this manuscript. We thank Thomas Kleinen and the two anonymous reviewers for their thorough reviews and insightful comments, which have greatly helped to improve the manuscript.

Chadburn, S. E., Burke, E. J., Gallego-Sala, A. V., Smith, N. D., Bret-Harte, M. S., Charman, D. J., et al. (2022). A new approach to simulate peat accumulation, degradation and stability in a global land surface scheme (JULES vn5.8_accumulate_soil) for northern and temperate peatlands. *Geoscientific Model Development*, *15*(4), 1633–1657. https://doi.org/10.5194/gmd-15-1633-2022

Chaudhary, N., Miller, P. A., & Smith, B. (2017). Modelling Holocene peatland dynamics with an individual-based dynamic vegetation model. *Biogeosciences*, *14*(10), 2571–2596. https://doi.org/10.5194/bg-14-2571-2017

Chen, J., & Chu, H. (2025). AmeriFlux FLUXNET-1F US-WPT winous point North Marsh (version 5–7) [Dataset]. *AmeriFlux AMP*. https://doi.org/10.17190/AMF/2229402

Cooper, D. J., & MacDonald, L. H. (2000). Restoring the vegetation of mined peatlands in the southern Rocky Mountains of Colorado, U.S.A. *Restoration Ecology*, *8*(2), 103–111. https://doi.org/10.1046/j.1526-100x.2000.80016.x

Desai, A. (2025). AmeriFlux BASE US-Los Lost Creek (version 3–5) [Dataset]. *AmeriFlux AMP*. https://doi.org/10.17190/AMF/1246071

Dickson-Hoyle, S., Stuxwtéws (Bonaparte First Nation), Skeetchestn Natural Resources Corporation, Eatherton, A., Baron, J. N., Tiribelli, F., & Daniels, L. D. (2024). Fire severity drives understory community dynamics and the recovery of culturally significant plants. *Ecosphere*, *15*(3), e4795. https://doi.org/10.1002/ecs2.4795

Dieleman, C. M., Branfireun, B. A., McLaughlin, J. W., & Lindo, Z. (2015). Climate change drives a shift in peatland ecosystem plant community: Implications for ecosystem function and stability. *Global Change Biology*, *21*(1), 388–395. https://doi.org/10.1111/gcb.12643

Druel, A., Ciais, P., Krinner, G., & Peylin, P. (2019). Modeling the vegetation dynamics of northern shrubs and mosses in the ORCHIDEE land surface model. *Journal of Advances in Modeling Earth Systems*, *11*(7), 2020–2035. https://doi.org/10.1029/2018MS001531

Druel, A., Peylin, P., Krinner, G., Ciais, P., Viovy, N., Peregon, A., et al. (2017). Towards a more detailed representation of high-latitude vegetation in the global land surface model ORCHIDEE (ORC-HL-VEGv1.0). *Geoscientific Model Development*, *10*(12), 4693–4722. https://doi.org/10.5194/gmd-10-4693-2017

Eichelmann, E., Shortt, R., Knox, S., Rey Sanchez, C., Valach, A., Sturtevant, C., et al. (2025). AmeriFlux FLUXNET-1F US-Tw4 Twitchell East End Wetland (version 5–7) [Dataset]. *AmeriFlux AMP*. https://doi.org/10.17190/AMF/2204881

Euskirchen, E. (2025a). AmeriFlux FLUXNET-1F US-BZB Bonanza Creek Thermokarst Bog (version 5–7) [Dataset]. *AmeriFlux AMP*. https://doi.org/10.17190/AMF/1881569

Euskirchen, E. (2025b). AmeriFlux FLUXNET-1F US-BZF Bonanza Creek Rich Fen (version 5–7) [Dataset]. *AmeriFlux AMP*. https://doi.org/10.17190/AMF/1881570

Euskirchen, E., Shaver, G., & Bret-Harte, S. (2025). AmeriFlux FLUXNET-1F US-ICs Imnavait Creek Watershed Wet Sedge Tundra (version 5–7) [Dataset]. *AmeriFlux AMP*. https://doi.org/10.17190/AMF/1871138

Flanagan, L. B. (2018). AmeriFlux BASE CA-WP1 Alberta—Western Peatland—LaBiche River, Black Spruce/Larch Fen (version 1–5) [Dataset]. *AmeriFlux AMP*. https://doi.org/10.17190/AMF/1436323

FLUXNET. (2015). FLUXNET2015 dataset [Dataset]. *FLUXNET Data Portal*. Retrieved from https://fluxnet.org/data/download-data/

Frolking, S., Roulet, N., & Lawrence, D. (2009). Issues related to incorporating northern peatlands into global climate models. In *Carbon Cycling in Northern Peatlands* (pp. 19–35). American Geophysical Union (AGU). https://doi.org/10.1029/2008GM000809

Frolking, S., & Roulet, N. T. (2007). Holocene radiative forcing impact of northern peatland carbon accumulation and methane emissions. *Global Change Biology*, *13*(5), 1079–1088. https://doi.org/10.1111/j.1365-2486.2007.01339.x

Frost, G. V., Bhatt, U. S., Macander, M. J., Berner, L. T., Walker, D. A., Raynolds, M. K., et al. (2025). The changing face of the Arctic: Four decades of greening and implications for tundra ecosystems. *Frontiers in Environmental Science*, *13*, 1525574. https://doi.org/10.3389/fenvs.2025.1525574

Gavazov, K., Albrecht, R., Buttler, A., Dorrepaal, E., Garnett, M. H., Gogo, S., et al. (2018). Vascular plant-mediated controls on atmospheric carbon assimilation and peat carbon decomposition under climate change. *Global Change Biology*, *24*(9), 3911–3921. https://doi.org/10.1111/gcb.14140

Goud, E. M., Moore, T. R., & Roulet, N. T. (2017). Predicting peatland carbon fluxes from non-destructive plant traits. *Functional Ecology*, *31*(9), 1824–1833. https://doi.org/10.1111/1365-2435.12891

Graham, J. A., Hartsock, J. A., Vitt, D. H., Wieder, R. K., & Gibson, J. J. (2016). Linkages between spatio-temporal patterns of environmental factors and distribution of plant assemblages across a boreal peatland complex. *Boreas*, *45*(2), 207–219. https://doi.org/10.1111/bor.12151

Griffiths, N. A., Sebestyen, S. D., & Oleheiser, K. C. (2019). Variation in peatland porewater chemistry over time and space along a bog to fen gradient. *Science of the Total Environment*, *697*, 134152. https://doi.org/10.1016/j.scitotenv.2019.134152

Guêné-Nanchen, M., LeBlanc, M.-C., & Rochefort, L. (2022). Post-fire peatland vegetation recovery: A case study in open rich fens of the Canadian boreal forest. *Botany*, *100*(5), 435–447. https://doi.org/10.1139/cjb-2021-0194

Harris, I., Osborn, T. J., Jones, P., & Lister, D. (2020). Version 4 of the CRU TS monthly high-resolution gridded multivariate climate dataset. *Scientific Data*, *7*(1), 109. https://doi.org/10.1038/s41597-020-0453-3

Heijmans, M. M., Mauquoy, D., Van Geel, B., & Berendse, F. (2008). Long-term effects of climate change on vegetation and carbon dynamics in peat bogs. *Journal of Vegetation Science*, *19*(3), 307–320. https://doi.org/10.3170/2008-8-18368

Hinkle, C. R., & Bracho, R. (2019). AmeriFlux BASE US-DPW Disney Wilderness Preserve Wetland (version 1–5) [Dataset]. *AmeriFlux AMP*. https://doi.org/10.17190/AMF/1562387

Hou, E., Ma, S., Huang, Y., Zhou, Y., Kim, H. S., López-Blanco, E., et al. (2023). Across-model spread and shrinking in predicting peatland carbon dynamics under global change. *Global Change Biology*, *29*(10), 2759–2775. https://doi.org/10.1111/gcb.16643

Hugelius, G., Loisel, J., Chadburn, S., Jackson, R. B., Jones, M., MacDonald, G., et al. (2020). Large stocks of peatland carbon and nitrogen are vulnerable to permafrost thaw. *Proceedings of the National Academy of Sciences of the United States of America*, *117*(34), 20438–20446. https://doi.org/10.1073/pnas.1916387117

Humphreys, E., & Lafleur, P. (2024). AmeriFlux BASE CA-Mer Ontario—Eastern Peatland, Mer Bleue (version 2–5) [Dataset]. *AmeriFlux AMP*. https://doi.org/10.17190/AMF/2448423

Hurtt, G. C., Chini, L. P., Frolking, S., Betts, R. A., Feddema, J., Fischer, G., et al. (2011). Harmonization of land-use scenarios for the period 1500–2100: 600 years of global gridded annual land-use transitions, wood harvest, and resulting secondary lands. *Climatic Change*, *109*(1), 117–161. https://doi.org/10.1007/s10584-011-0153-2

Jassey, V. E. J., Reczuga, M. K., Zielińska, M., Słowińska, S., Robroek, B. J. M., Mariotte, P., et al. (2018). Tipping point in plant–fungal interactions under severe drought causes abrupt rise in peatland ecosystem respiration. *Global Change Biology*, *24*(3), 972–986. https://doi.org/10.1111/gcb.13928

Jeong, S., Ryu, Y., Gentine, P., Lian, X., Fang, J., Li, X., et al. (2024). Persistent global greening over the last four decades using novel long-term vegetation index data with enhanced temporal consistency. *Remote Sensing of Environment*, *311*, 114282. https://doi.org/10.1016/j.rse.2024.114282

Jian, J., Bailey, V., Dorheim, K., Konings, A. G., Hao, D., Shiklomanov, A. N., et al. (2022). Historically inconsistent productivity and respiration fluxes in the global terrestrial carbon cycle. *Nature Communications*, *13*(1), 1733. https://doi.org/10.1038/s41467-022-29391-5

Jones, E., Chasmer, L., Devito, K., Rood, S., & Hopkinson, C. (2022). Ecological impacts of shortening fire return intervals on boreal peatlands and transition zones using integrated in situ field sampling and LiDAR approaches. *Ecohydrology*, *15*(3), e2403. https://doi.org/10.1002/eco.2403

Kalhori, A., Wille, C., Gottschalk, P., Li, Z., Hashemi, J., Kemper, K., & Sachs, T. (2024). Temporally dynamic carbon dioxide and methane emission factors for rewetted peatlands. *Communications Earth & Environment*, *5*(1), 1–11. https://doi.org/10.1038/s43247-024-01226-9

Karlson, M., & Bastviken, D. (2023). Multi-source mapping of peatland types using Sentinel-1, Sentinel-2, and Terrain Derivatives—A comparison between five high-latitude landscapes. *Journal of Geophysical Research: Biogeosciences*, *128*(4), e2022JG007195. https://doi.org/10.1029/2022JG007195

Kleinen, T., Brovkin, V., & Schuldt, R. J. (2012). A dynamic model of wetland extent and peat accumulation: Results for the Holocene. *Biogeosciences*, *9*(1), 235–248. https://doi.org/10.5194/bg-9-235-2012

Kobayashi, S., Ota, Y., Harada, Y., Ebita, A., Moriya, M., Onoda, H., et al. (2015). The JRA-55 reanalysis: General specifications and basic characteristics. *Journal of the Meteorological Society of Japan. Series II*, *93*(1), 5–48. https://doi.org/10.2151/jmsj.2015-001

Krinner, G., Viovy, N., de Noblet-Ducoudré, N., Ogée, J., Polcher, J., Friedlingstein, P., et al. (2005). A dynamic global vegetation model for studies of the coupled atmosphere-biosphere system. *Global Biogeochemical Cycles*, *19*(1). https://doi.org/10.1029/2003GB002199

Kwon, M. J., Ballantyne, A., Ciais, P., Qiu, C., Salmon, E., Raoult, N., et al. (2022). Lowering water table reduces carbon sink strength and carbon stocks in northern peatlands. *Global Change Biology*, *28*(22), 6752–6770. https://doi.org/10.1111/gcb.16394

Largeron, C., Krinner, G., Ciais, P., & Brutel-Vuilmet, C. (2018). Implementing northern peatlands in a global land surface model: Description and evaluation in the ORCHIDEE high-latitude version model (ORC-HL-PEAT). *Geoscientific Model Development*, *11*(8), 3279–3297. https://doi.org/10.5194/gmd-11-3279-2018

Lasslop, G., Reichstein, M., Papale, D., Richardson, A. D., Arneth, A., Barr, A., et al. (2010). Separation of net ecosystem exchange into assimilation and respiration using a light response curve approach: Critical issues and global evaluation. *Global Change Biology*, *16*(1), 187–208. https://doi.org/10.1111/j.1365-2486.2009.02041.x

Leifeld, J., & Menichetti, L. (2018). The underappreciated potential of peatlands in global climate change mitigation strategies. *Nature Communications*, *9*(1), 1071. https://doi.org/10.1038/s41467-018-03406-6

Li, X., & Xiao, J. (2019). Mapping photosynthesis solely from solar-induced chlorophyll fluorescence: A global, fine-resolution dataset of gross primary production derived from OCO-2. *Remote Sensing*, *11*(21), 2563. https://doi.org/10.3390/rs11212563

Liang, S., Cheng, J., Jia, K., Jiang, B., Liu, Q., Xiao, Z., et al. (2021). The Global Land Surface Satellite (GLASS) product suite. https://doi.org/10.1175/BAMS-D-18-0341.1

Liu, Y., Liu, R., & Chen, J. M. (2012). Retrospective retrieval of long-term consistent global leaf area index (1981–2011) from combined AVHRR and MODIS data. *Journal of Geophysical Research*, *117*(G4). https://doi.org/10.1029/2012JG002084

López-Blanco, E., Topp-Jørgensen, E., Christensen, T. R., Rasch, M., Skov, H., Arndal, M. F., et al. (2024). Towards an increasingly biased view on Arctic change. *Nature Climate Change*, *14*(2), 152–155. https://doi.org/10.1038/s41558-023-01903-1

Matthes, J. H., Sturtevant, C., Oikawa, P., Chamberlain, S. D., Szutu, D., Arias-Ortiz, A., et al. (2022). AmeriFlux FLUXNET-1F US-Myb Mayberry Wetland (version 3–5) [Dataset]. *AmeriFlux AMP*. https://doi.org/10.17190/AMF/1871139

McPartland, M. Y., Montgomery, R. A., Hanson, P. J., Phillips, J. R., Kolka, R., & Palik, B. (2020). Vascular plant species response to warming and elevated carbon dioxide in a boreal peatland. *Environmental Research Letters*, *15*(12), 124066. https://doi.org/10.1088/1748-9326/abc4fb

Mekonnen, Z. A., Riley, W. J., Berner, L. T., Bouskill, N. J., Torn, M. S., Iwahana, G., et al. (2021). Arctic tundra shrubification: A review of mechanisms and impacts on ecosystem carbon balance. *Environmental Research Letters*, *16*(5), 053001. https://doi.org/10.1088/1748-9326/abf28b

Mualem, Y. (1976). A new model for predicting the hydraulic conductivity of unsaturated porous media. *Water Resources Research*, *12*(3), 513–522. https://doi.org/10.1029/WR012i003p00513

Müller, J., & Joos, F. (2020). Global peatland area and carbon dynamics from the Last Glacial Maximum to the present—A process-based model investigation. *Biogeosciences*, *17*(21), 5285–5308. https://doi.org/10.5194/bg-17-5285-2020

Myers-Smith, I. H., Kerby, J. T., Phoenix, G. K., Bjerke, J. W., Epstein, H. E., Assmann, J. J., et al. (2020). Complexity revealed in the greening of the Arctic. *Nature Climate Change*, *10*(2), 106–117. https://doi.org/10.1038/s41558-019-0688-1

Nelson, J. A., Walther, S., Gans, F., Kraft, B., Weber, U., Novick, K., et al. (2024). X-BASE: The first terrestrial carbon and water flux products from an extended data-driven scaling framework, FLUXCOM-X. *Biogeosciences*, *21*(22), 5079–5115. https://doi.org/10.5194/bg-21-5079-2024

Norby, R. J., Childs, J., Hanson, P. J., & Warren, J. M. (2019). Rapid loss of an ecosystem engineer: Sphagnum decline in an experimentally warmed bog. *Ecology and Evolution*, *9*(22), 12571–12585. https://doi.org/10.1002/ece3.5722

Nuyim, T. (2000). Whole aspect on nature and management of peat swamp forest in Thailand. In *Proceedings of the International Symposium on Tropical Peatlands* (pp. 109–117). Bogor. Retrieved from http://www.ees.hokudai.ac.jp/coe21/E/indonesia/trpt99_3.pdf

Olefeldt, D., Hovemyr, M., Kuhn, M. A., Bastviken, D., Bohn, T. J., Connolly, J., et al. (2021). The Boreal–Arctic wetland and lake dataset (BAWLD). *Earth System Science Data*, *13*(11), 5127–5149. https://doi.org/10.5194/essd-13-5127-2021

Peltola, O., Vesala, T., Gao, Y., Räty, O., Alekseychik, P., Aurela, M., et al. (2019). Monthly gridded data product of northern wetland methane emissions based on upscaling eddy covariance observations. *Earth System Science Data*, *11*(3), 1263–1289. https://doi.org/10.5194/essd-11-1263-2019

Peregon, A., Maksyutov, S., Kosykh, N. P., & Mironycheva-Tokareva, N. P. (2008). Map-based inventory of wetland biomass and net primary production in western Siberia. *Journal of Geophysical Research*, *113*(G1). https://doi.org/10.1029/2007JG000441

Peregon, A., Maksyutov, S., & Yamagata, Y. (2009). An image-based inventory of the spatial structure of West Siberian wetlands. *Environmental Research Letters*, *4*(4), 045014. https://doi.org/10.1088/1748-9326/4/4/045014

Piao, S., Wang, X., Park, T., Chen, C., Lian, X., He, Y., et al. (2020). Characteristics, drivers and feedbacks of global greening. *Nature Reviews Earth & Environment*, *1*(1), 14–27. https://doi.org/10.1038/s43017-019-0001-x

Qiu, C. (2026a). ORCHIDEE-PEAT: Modelling sub-grid peatland vegetation dynamics [Software]. *Zenodo*. https://doi.org/10.5281/zenodo.18241888

Qiu, C. (2026b). Model outputs presented in the JAMES paper: Modelling sub-grid peatland vegetation dynamics in the ORCHIDEE-PEAT land surface model [Dataset]. *Zenodo*. https://doi.org/10.5281/zenodo.18382534

Qiu, C., Ciais, P., Zhu, D., Guenet, B., Chang, J., Chaudhary, N., et al. (2022). A strong mitigation scenario maintains climate neutrality of northern peatlands. *One Earth*, *5*(1), 86–97. https://doi.org/10.1016/j.oneear.2021.12.008

Qiu, C., Ciais, P., Zhu, D., Guenet, B., Peng, S., Petrescu, A. M. R., et al. (2021). Large historical carbon emissions from cultivated northern peatlands. *Science Advances*, *7*(23), eabf1332. https://doi.org/10.1126/sciadv.abf1332

Qiu, C., Zhu, D., Ciais, P., Guenet, B., Krinner, G., Peng, S., et al. (2018). ORCHIDEE-PEAT (revision 4596), a model for northern peatland CO_2, water, and energy fluxes on daily to annual scales. *Geoscientific Model Development*, *11*(2), 497–519. https://doi.org/10.5194/gmd-11-497-2018

Qiu, C., Zhu, D., Ciais, P., Guenet, B., Peng, S., Krinner, G., et al. (2019). Modelling northern peatland area and carbon dynamics since the Holocene with the ORCHIDEE-PEAT land surface model (SVN r5488). *Geoscientific Model Development*, *12*(7), 2961–2982. https://doi.org/10.5194/gmd-12-2961-2019

Rantanen, M., Karpechko, A. Y., Lipponen, A., Nordling, K., Hyvärinen, O., Ruosteenoja, K., et al. (2022). The Arctic has warmed nearly four times faster than the globe since 1979. *Communications Earth & Environment*, *3*(1), 1–10. https://doi.org/10.1038/s43247-022-00498-3

Räsänen, A., Aurela, M., Juutinen, S., Kumpula, T., Lohila, A., Penttilä, T., & Virtanen, T. (2020). Detecting northern peatland vegetation patterns at ultra-high spatial resolution. *Remote Sensing in Ecology and Conservation*, *6*(4), 457–471. https://doi.org/10.1002/rse2.140

Ratcliffe, J. L., Campbell, D. I., Clarkson, B. R., Wall, A. M., & Schipper, L. A. (2019). Water table fluctuations control CO_2 exchange in wet and dry bogs through different mechanisms. *Science of the Total Environment*, *655*, 1037–1046. https://doi.org/10.1016/j.scitotenv.2018.11.151

Ratcliffe, J. L., Campbell, D. I., Schipper, L. A., Wall, A. M., & Clarkson, B. R. (2020). Recovery of the CO_2 sink in a remnant peatland following water table lowering. *Science of the Total Environment*, *718*, 134613. https://doi.org/10.1016/j.scitotenv.2019.134613

Reichstein, M., Falge, E., Baldocchi, D., Papale, D., Aubinet, M., Berbigier, P., et al. (2005). On the separation of net ecosystem exchange into assimilation and ecosystem respiration: Review and improved algorithm. *Global Change Biology*, *11*(9), 1424–1439. https://doi.org/10.1111/j.1365-2486.2005.001002.x

Ribeiro, K., Pacheco, F. S., Ferreira, J. W., de Sousa-Neto, E. R., Hastie, A., Krieger Filho, G. C., et al. (2021). Tropical peatlands and their contribution to the global carbon cycle and climate change. *Global Change Biology*, *27*(3), 489–505. https://doi.org/10.1111/gcb.15408

Robroek, B. J. M., Jassey, V. E. J., Payne, R. J., Martí, M., Bragazza, L., Bleeker, A., et al. (2017). Taxonomic and functional turnover are decoupled in European peat bogs. *Nature Communications*, *8*(1), 1161. https://doi.org/10.1038/s41467-017-01350-5

Salmon, E., Jégou, F., Guenet, B., Jourdain, L., Qiu, C., Bastrikov, V., et al. (2022). Assessing methane emissions for northern peatlands in ORCHIDEE-PEAT revision 7020. *Geoscientific Model Development*, *15*(7), 2813–2838. https://doi.org/10.5194/gmd-15-2813-2022

Schipper, L. A., Clarkson, B. R., Vojvodic-Vukovic, M., & Webster, R. (2002). Restoring cut-over restiad peat bogs: A factorial experiment of nutrients, seed and cultivation. *Ecological Engineering*, *19*(1), 29–40. https://doi.org/10.1016/S0925-8574(02)00013-7

Shepherd, H. E. R., Catford, J. A., Steele, M. N., Dumont, M. G., Mills, R. T. E., Hughes, P. D. M., & Robroek, B. J. M. (2021). Propagule availability drives post-wildfire recovery of peatland plant communities. *Applied Vegetation Science*, *24*(3), e12608. https://doi.org/10.1111/avsc.12608

Shi, X., Ricciuto, D. M., Thornton, P. E., Xu, X., Yuan, F., Norby, R. J., et al. (2021). Extending a land-surface model with Sphagnum moss to simulate responses of a northern temperate bog to whole ecosystem warming and elevated CO_2. *Biogeosciences*, *18*(2), 467–486. https://doi.org/10.5194/bg-18-467-2021

Shortt, R., Hemes, K., Szutu, D., Verfaillie, J., & Baldocchi, D. (2025). AmeriFlux FLUXNET-1F US-Sne Sherman Island Restored Wetland (version 5–7) [Dataset]. *AmeriFlux AMP*. https://doi.org/10.17190/AMF/1871144

Sitch, S., Smith, B., Prentice, I. C., Arneth, A., Bondeau, A., Cramer, W., et al. (2003). Evaluation of ecosystem dynamics, plant geography and terrestrial carbon cycling in the LPJ dynamic global vegetation model. *Global Change Biology*, *9*(2), 161–185. https://doi.org/10.1046/j.1365-2486.2003.00569.x

Smith, B., Prentice, I. C., & Sykes, M. T. (2001). Representation of vegetation dynamics in the modelling of terrestrial ecosystems: Comparing two contrasting approaches within European climate space. *Global Ecology and Biogeography*, *10*(6), 621–637. https://doi.org/10.1046/j.1466-822X.2001.t01-1-00256.x

Sonnentag, O., & Quinton, W. L. (2025). AmeriFlux FLUXNET-1F CA-SCB Scotty Creek Bog (version v1.3_r1) [Dataset]. *AmeriFlux AMP*. https://doi.org/10.17190/AMF/2469439

Spahni, R., Joos, F., Stocker, B. D., Steinacher, M., & Yu, Z. C. (2013). Transient simulations of the carbon and nitrogen dynamics in northern peatlands: From the Last Glacial Maximum to the 21st century. *Climate of the Past*, *9*(3), 1287–1308. https://doi.org/10.5194/cp-9-1287-2013

Stocker, B. D., Spahni, R., & Joos, F. (2014). DYPTOP: A cost-efficient TOPMODEL implementation to simulate sub-grid spatio-temporal dynamics of global wetlands and peatlands. *Geoscientific Model Development*, *7*(6), 3089–3110. https://doi.org/10.5194/gmd-7-3089-2014

Sullivan, R., Billesbach, D., Cook, D., & Biraud, S. (2025). AmeriFlux BASE US-A10 ARM-NSA-Barrow (version 5–5) [Dataset]. *AmeriFlux AMP*. https://doi.org/10.17190/AMF/1498753

Sulman, B. N., Desai, A. R., & Mladenoff, D. J. (2013). Modeling soil and biomass carbon responses to declining water table in a wetland-rich landscape. *Ecosystems*, *16*(3), 491–507. https://doi.org/10.1007/s10021-012-9624-1

Swindles, G. T., Morris, P. J., Mullan, D. J., Payne, R. J., Roland, T. P., Amesbury, M. J., et al. (2019). Widespread drying of European peatlands in recent centuries. *Nature Geoscience*, *12*(11), 922–928. https://doi.org/10.1038/s41561-019-0462-z

Temmink, R. J. M., Cruijsen, P. M. J. M., Smolders, A. J. P., Bouma, T. J., Fivash, G. S., Lengkeek, W., et al. (2021). Overcoming establishment thresholds for peat mosses in human-made bog pools. *Ecological Applications*, *31*(6), e02359. https://doi.org/10.1002/eap.2359

Thompson, D. K., Simpson, B. N., & Beaudoin, A. (2016). Using forest structure to predict the distribution of treed boreal peatlands in Canada. *Forest Ecology and Management*, *372*, 19–27. https://doi.org/10.1016/j.foreco.2016.03.056

Torn, M., & Dengel, S. (2025a). AmeriFlux FLUXNET-1F US-NGC NGEE Arctic Council (version 5–7) [Dataset]. *AmeriFlux AMP*. https://doi.org/10.17190/AMF/1902838

Torn, M., & Dengel, S. (2025b). AmeriFlux FLUXNET-1F US-NGB NGEE Arctic Barrow (version 4–7) [Dataset]. *AmeriFlux AMP*. https://doi.org/10.17190/AMF/1832162

Triisberg, T., Karofeld, E., & Paal, J. (2011). Re-vegetation of block-cut and milled peatlands: An Estonian example. *Mires & Peat*, *8*. https://doi.org/10.19189/001c.128432

Turetsky, M. R., Bond-Lamberty, B., Euskirchen, E., Talbot, J., Frolking, S., McGuire, A. D., & Tuittila, E.-S. (2012). The resilience and functional role of moss in boreal and arctic ecosystems. *New Phytologist*, *196*(1), 49–67. https://doi.org/10.1111/j.1469-8137.2012.04254.x

Ueyama, M., Iwata, H., & Harazono, Y. (2025). AmeriFlux BASE US-Uaf University of Alaska, Fairbanks (version 14–5) [Dataset]. *AmeriFlux AMP*. https://doi.org/10.17190/AMF/1480322

Valach, A., Kasak, K., Szutu, D., Verfaillie, J., & Baldocchi, D. (2025). AmeriFlux FLUXNET-1F US-Tw5 East Pond Wetland (version 5–7) [Dataset]. *AmeriFlux AMP*. https://doi.org/10.17190/AMF/1881595

Valach, A., Shortt, R., Szutu, D., Eichelmann, E., Knox, S., Hemes, K., et al. (2025). AmeriFlux FLUXNET-1F US-Tw1 Twitchell Wetland West Pond (version 5–7) [Dataset]. *AmeriFlux AMP*. https://doi.org/10.17190/AMF/1832165

Van Genuchten, M. T. (1980). A closed-form equation for predicting the hydraulic conductivity of unsaturated soils. *Soil Science Society of America Journal*, *44*(5), 892–898. https://doi.org/10.2136/sssaj1980.03615995004400050002x

Virkkala, A. M., Aalto, J., Rogers, B. M., Tagesson, T., Treat, C. C., Natali, S. M., et al. (2021). Statistical upscaling of ecosystem CO_2 fluxes across the terrestrial tundra and boreal domain: Regional patterns and uncertainties. *Global Change Biology*, *27*(17), 4040–4059. https://doi.org/10.1111/gcb.15659

Virkkala, A. M., Natali, S. M., Rogers, B. M., Watts, J. D., Savage, K., Connon, S. J., et al. (2022). The ABCflux database: Arctic-boreal CO_2 flux observations and ancillary information aggregated to monthly time steps across terrestrial ecosystems. *Earth System Science Data Discussions*, *14*(1), 179–208. https://doi.org/10.5194/essd-14-179-2022

Vourlitis, G. L., Dalmagro, H., Nogueira, J. S., Johnson, M., & Arruda, P. (2025). AmeriFlux FLUXNET-1F BR-Npw Northern Pantanal Wetland (version 5–7) [Dataset]. *AmeriFlux AMP*. https://doi.org/10.17190/AMF/1881563

Walker, T. N., Garnett, M. H., Ward, S. E., Oakley, S., Bardgett, R. D., & Ostle, N. J. (2016). Vascular plants promote ancient peatland carbon loss with climate warming. *Global Change Biology*, *22*(5), 1880–1889. https://doi.org/10.1111/gcb.13213

Wang, H., Richardson, C. J., & Ho, M. (2015). Dual controls on carbon loss during drought in peatlands. *Nature Climate Change*, *5*(6), 584–587. https://doi.org/10.1038/nclimate2643

Wang, H., Tian, J., Chen, H., Ho, M., Vilgalys, R., Bu, Z.-J., et al. (2021). Vegetation and microbes interact to preserve carbon in many wooded peatlands. *Communications Earth & Environment*, *2*(1), 1–8. https://doi.org/10.1038/s43247-021-00136-4

Wania, R., Ross, I., & Prentice, I. C. (2009). Integrating peatlands and permafrost into a dynamic global vegetation model: 1. Evaluation and sensitivity of physical land surface processes. *Global Biogeochemical Cycles*, *23*(3). https://doi.org/10.1029/2008GB003412

Warm Winter 2020 Team, ICOS Ecosystem Thematic Centre. (2022). Warm winter 2020 ecosystem eddy covariance flux product for 73 stations in FLUXNET-Archive format-release 2022-1. https://doi.org/10.18160/2G60-ZHAK

Ward, E., Merino, S., Stagg, C., & Krauss, K. (2025). AmeriFlux BASE US-LA2 Salvador WMA Freshwater Marsh (version 4–5) [Dataset]. *AmeriFlux AMP*. https://doi.org/10.17190/AMF/1543387

Weltzin, J. F., Bridgham, S. D., Pastor, J., Chen, J., & Harth, C. (2003). Potential effects of warming and drying on peatland plant community composition. *Global Change Biology*, *9*(2), 141–151. https://doi.org/10.1046/j.1365-2486.2003.00571.x

Weltzin, J. F., Pastor, J., Harth, C., Bridgham, S. D., Updegraff, K., & Chapin, C. T. (2000). Response of bog and fen plant communities to warming and water-table manipulations. *Ecology*, *81*(12), 3464–3478. https://doi.org/10.1890/0012-9658(2000)081[3464:ROBAFP]2.0.CO;2

Whitehead, J., Wittemann, M., & Cronberg, N. (2018). Allelopathy in bryophytes—A review. *Lindbergia*, *41*(1). https://doi.org/10.25227/linbg.01097

Xiao, Z., Liang, S., Wang, J., Xiang, Y., Zhao, X., & Song, J. (2016). Long-time-series global land surface satellite leaf area index product derived from MODIS and AVHRR surface reflectance. *IEEE Transactions on Geoscience and Remote Sensing*, *54*(9), 5301–5318. https://doi.org/10.1109/TGRS.2016.2560522

Xu, J., Morris, P. J., Liu, J., & Holden, J. (2018). PEATMAP: Refining estimates of global peatland distribution based on a meta-analysis. *Catena*, *160*, 134–140. https://doi.org/10.1016/j.catena.2017.09.010

Yue, C., Ciais, P., Cadule, P., Thonicke, K., Archibald, S., Poulter, B., et al. (2014). Modelling the role of fires in the terrestrial carbon balance by incorporating SPITFIRE into the global vegetation model ORCHIDEE—Part 1: Simulating historical global burned area and fire regimes. *Geoscientific Model Development*, *7*(6), 2747–2767. https://doi.org/10.5194/gmd-7-2747-2014

Yue, C., Ciais, P., Cadule, P., Thonicke, K., & Van Leeuwen, T. T. (2015). Modelling the role of fires in the terrestrial carbon balance by incorporating SPITFIRE into the global vegetation model ORCHIDEE—Part 2: Carbon emissions and the role of fires in the global carbon balance. *Geoscientific Model Development*, *8*(5), 1321–1338. https://doi.org/10.5194/gmd-8-1321-2015

Zanaga, D., Van De Kerchove, R., Daems, D., De Keersmaecker, W., Brockmann, C., Kirches, G., et al. (2022). ESA WorldCover 10 m 2021 v200 (version v200) [Dataset]. *Zenodo*. https://doi.org/10.5281/zenodo.7254221

Zhang, H., Väliranta, M., Swindles, G. T., Aquino-López, M. A., Mullan, D., Tan, N., et al. (2022). Recent climate change has driven divergent hydrological shifts in high-latitude peatlands. *Nature Communications*, *13*(1), 4959. https://doi.org/10.1038/s41467-022-32711-4

Zhang, Y., Xiao, X., Wu, X., Zhou, S., Zhang, G., Qin, Y., & Dong, J. (2017). A global moderate resolution dataset of gross primary production of vegetation for 2000–2016. *Scientific Data*, *4*(1), 170165. https://doi.org/10.1038/sdata.2017.165

Zhao, B., & Zhuang, Q. (2023). Peatlands and their carbon dynamics in northern high latitudes from 1990 to 2300: A process-based biogeochemistry model analysis. *Biogeosciences*, *20*(1), 251–270. https://doi.org/10.5194/bg-20-251-2023

Zhao, J., Weldon, S., Barthelmes, A., Swails, E., Hergoualc'h, K., Mander, Ü., et al. (2024). Global observation gaps of peatland greenhouse gas balances: Needs and obstacles. *Biogeochemistry*, *167*(4), 427–442. https://doi.org/10.1007/s10533-023-01091-2

Zhu, D., Peng, S. S., Ciais, P., Viovy, N., Druel, A., Kageyama, M., et al. (2015). Improving the dynamics of Northern Hemisphere high-latitude vegetation in the ORCHIDEE ecosystem model. *Geoscientific Model Development*, *8*(7), 2263–2283. https://doi.org/10.5194/gmd-8-2263-2015

Zhu, Z., Piao, S., Myneni, R. B., Huang, M., Zeng, Z., Canadell, J. G., et al. (2016). Greening of the Earth and its drivers. *Nature Climate Change*, *6*(8), 791–795. https://doi.org/10.1038/nclimate3004

Zona, D., & Oechel, W. (2016). AmeriFlux BASE US-Atq Atqasuk (version 1–1) [Dataset]. *AmeriFlux AMP*. https://doi.org/10.17190/AMF/1246029

Zona, D., & Oechel, W. (2019). AmeriFlux BASE US-Ivo Ivotuk (version 4–5) [Dataset]. *AmeriFlux AMP*. https://doi.org/10.17190/AMF/1246067